Influence of Seed Aerosol Surface Area and Oxidation Rate on Vapor-Wall Deposition and SOA Mass Yields: A case study with α-pinene Ozonolysis

T. Nah,[1] R. C. McVay,[2] X. Zhang,[3,#] C. M. Boyd,[1] J. H. Seinfeld[2,3] and N. L. Ng[1,4*]

[1]*School of Chemical and Biomolecular Engineering, Georgia Institute of Technology, Atlanta, GA, USA*
[2]*Division of Chemistry and Chemical Engineering, California Institute of Technology, Pasadena, CA, USA*
[3]*Division of Engineering and Applied Science, California Institute of Technology, Pasadena, CA, USA*
[4]*School of Earth and Atmospheric Sciences, Georgia Institute of Technology, Atlanta, GA, USA*
[#]*Now at: Center for Aerosol and Cloud Chemistry, Aerodyne Research, Billerica, MA, USA*

** To whom correspondence should be addressed: ng@chbe.gatech.edu*

Abstract

Laboratory chambers, invaluable in atmospheric chemistry and aerosol formation studies, are subject to particle and vapor wall deposition, processes that need to be accounted for in order to accurately determine secondary organic aerosol (SOA) mass yields. Although particle wall deposition is reasonably well understood and usually accounted for, vapor wall deposition is less so. The effects of vapor wall deposition on SOA mass yields in chamber experiments can be constrained experimentally by increasing the seed aerosol surface area to promote the preferential condensation of SOA-forming vapors onto seed aerosol. Here, we study the influence of seed aerosol surface area and oxidation rate on SOA formation in α-pinene ozonolysis. The observations are analyzed using a coupled vapor-particle dynamics model to interpret the roles of gas-particle partitioning (quasi-equilibrium vs. kinetically-limited SOA growth) and α-pinene oxidation rate in influencing vapor wall deposition. We find that the SOA growth rate and mass yields are independent of seed surface area within the range of seed surface area concentrations used in this study. This behavior arises when the condensation of SOA-forming vapors is dominated by quasi-equilibrium growth. Faster α-pinene oxidation rates and higher SOA mass yields are observed at increasing O_3 concentrations for the same initial α-pinene concentration. When the α-pinene oxidation rate increases relative to vapor wall deposition, rapidly produced SOA-forming oxidation products condense more readily onto seed aerosol particles, resulting in higher SOA mass yields. Our results indicate that the extent to which vapor wall deposition affects SOA mass yields depends on the

particular VOC system, and can be mitigated through the use of excess oxidant concentrations.

1. Introduction

Secondary organic aerosol (SOA), formed from the oxidation of volatile and intermediate volatility organic compounds (VOCs and IVOCs), contributes a significant fraction of the global organic aerosol burden (Kanakidou et al., 2005; Hallquist et al., 2009; Tsigaridis et al., 2014). SOA formation studies, which are typically conducted in laboratory chambers in the presence of seed aerosol particles, provide fundamental data that can be used to predict the rate of atmospheric SOA formation. An essential parameter of interest in laboratory chamber studies is the SOA mass yield (Y), which is defined as the ratio of mass concentration of SOA formed to mass concentration of parent hydrocarbon reacted ((ΔHC), $Y = \Delta M_o/\Delta HC$ (Odum et al., 1996; Odum et al., 1997a; Odum et al., 1997b)). The measured SOA mass yields can subsequently be applied in atmospheric models to predict regional and global organic aerosol burdens. In order to obtain accurate SOA mass yields from the evolving aerosol size distribution in chamber experiments, the loss of both particles and vapors to the chamber walls needs to be accurately accounted for (Crump and Seinfeld, 1981; McMurry and Grosjean, 1985; McMurry and Rader, 1985; Cocker et al., 2001a; Weitkamp et al., 2007; Pierce et al., 2008; Hildebrandt et al., 2009; Loza et al., 2010; Matsunaga and Ziemann, 2010; Loza et al., 2012; Kokkola et al., 2014; McVay et al., 2014; Yeh and Ziemann, 2014; Zhang et al., 2014; Yeh and Ziemann, 2015; Zhang et al., 2015a; La et al., 2016; Ye et al., 2016).

The mechanisms by which particles in chambers deposit on chamber walls are reasonably well understood. Particles are transported to the boundary layer on the chamber walls via diffusion, gravitational settling, and electrostatic forces (Crump and Seinfeld, 1981; McMurry and Grosjean, 1985; McMurry and Rader, 1985; Pierce et al., 2008). The rate at which particles are transported to the edge of the boundary layer is dictated primarily by mixing conditions in the chamber. An effective approach for characterizing particle wall loss involves measuring the size-dependent wall loss rates of polydisperse inert seed aerosol (e.g. ammonium sulfate particles) injected into the chamber during seed-only experiments (Keywood et al., 2004; Pierce et al., 2008). The

observed particle number concentration decay in each size bin is then fitted to a first-order exponential decay from which the first-order wall loss coefficients are determined as a function of particle size. These wall loss coefficients are subsequently used to correct for size-dependent particle wall loss in actual SOA formation experiments. Determination of particle wall loss coefficients may be complicated if coagulation is significant. Particle dynamics models can be used to correct particle wall loss coefficients for coagulation.

Vapor-wall deposition mechanisms in chambers are not as well understood or accounted for as those for particles. The degree to which SOA-forming vapors deposit onto chamber walls is governed by the rate at which these gas-phase organic molecules are transported to the walls, the strength of adherence of the organic molecule to the wall, and the extent of reversible vapor-wall partitioning (Loza et al., 2010; Matsunaga and Ziemann, 2010; Zhang et al., 2015a). For example, Loza et al. (2010) showed that the loss of 2,3-epoxy-1,4-butanediol, an isoprene oxidation product analogue, to walls in the Caltech chamber was essentially irreversible on short time scales but became reversible on longer time scales. In contrast, glyoxal, a common isoprene oxidation product, exhibited reversible vapor-wall partitioning over all time scales. Recent studies show that SOA mass yields measured in chamber experiments can be significantly underestimated due to wall deposition of SOA-forming vapors that would otherwise contribute to SOA growth (McVay et al., 2014; Zhang et al., 2014; La et al., 2016). Zhang et al. (2014) found that chamber-derived SOA mass yields from toluene photooxidation may be underestimated by as much as a factor of four as a result of vapor wall loss. Consequently, the use of underestimated chamber-derived SOA mass yields in atmospheric models will lead to the underprediction of ambient SOA mass concentrations (Cappa et al., 2016).

For the toluene photooxidation system, Zhang et al. (2014) showed that the measured SOA mass yields increased with increasing seed aerosol surface area, demonstrating that increasing the seed-to-chamber surface area ratio promoted the condensation of SOA-forming vapors onto seed aerosol particles. However, increasing the seed aerosol surface area to promote condensation of SOA-forming vapors onto seed aerosol particles may not be effective in all VOC oxidation systems. A modeling study by

McVay et al. (2014) showed that the SOA mass yield depends on seed aerosol surface area only in cases where the condensation of SOA-forming vapors onto seed aerosol particles is kinetically limited (i.e., the timescale for gas-particle equilibrium is competitive with or greater than the timescale for reaction and vapor-wall deposition). In addition to the seed aerosol surface area, VOC oxidation rate may also play an important role in the effect of vapor wall loss on SOA formation. Ng et al. (2007) showed that the SOA mass yields from *m*-xylene photooxidation are dependent on the oxidation rate, with higher OH concentrations (hence faster oxidation rates) resulting in higher SOA mass yields. It was suggested that the "oxidation rate effect" could arise as a result of competition between growing particles and chamber walls for condensable VOC oxidation products (Ng et al., 2007). However, McVay et al. (2016) reported similar SOA growth at low and high OH concentrations in α-pinene photooxidation. Taken together, these studies show the importance of understanding how gas-particle partitioning and VOC oxidation rate impact vapor-wall deposition and SOA mass yields in laboratory chamber experiments.

In this study, we examine the influence of seed aerosol surface area and oxidation rate on SOA formation in α-pinene ozonolysis chamber experiments. α-pinene is the most abundant monoterpene, with global emissions estimated to be ~66 Tg yr^{-1} (Guenther et al., 2012). Ozonolysis is the major atmospheric oxidation pathway of α-pinene, and is estimated to account for reaction of ~46 % of emitted α-pinene (Griffin et al., 1999; Capouet et al., 2008). α-pinene ozonolysis, a major source of atmospheric SOA on both regional and global scales (Kanakidou et al., 2005; Hallquist et al., 2009; Carlton et al., 2010; Pye et al., 2010), has been the subject of numerous studies (Hoffmann et al., 1997; Griffin et al., 1999; Cocker et al., 2001b; Gao et al., 2004; Presto et al., 2005; Presto and Donahue, 2006; Pathak et al., 2007a; Pathak et al., 2007b; Song et al., 2007; Shilling et al., 2008; Henry et al., 2012; Ehn et al., 2014; Kristensen et al., 2014; Zhang et al., 2015b). Here, we measure the α-pinene SOA mass yield as a function of seed aerosol surface area concentration (0 to 3000 μm^2 cm^{-3}) and O_3 mixing ratio (100 vs. 500 ppb). These results are analyzed using a coupled vapor-particle dynamics model to evaluate the roles of gas-particle partitioning and VOC oxidation rate in influencing vapor-wall deposition effects on the measured SOA mass yields.

2. Experimental

2.1. Dark α-pinene ozonolysis experiments

Experiments were conducted in the Georgia Tech Environmental Chamber (GTEC) facility. Details of the dual chamber facility are provided elsewhere (Boyd et al., 2015). Only one FEP Teflon chamber (volume 13 m^3) was used for the entirety of this study. Before each experiment, the chamber was flushed with dried, purified air for at least 36 h until the aerosol number concentration was < 30 cm^{-3}. All experiments were conducted under dry conditions (< 5 % RH) at room temperature (25 °C). NO_x mixing ratios in these experiments were < 1 ppb. Experimental conditions are summarized in Table 1.

22 ppm of cyclohexane (Sigma Aldrich, ≥ 99.9 %) was first injected into the chamber to act as an OH scavenger (~440 times the initial α-pinene concentration). Based on the concentrations of cyclohexane and α-pinene injected into the chamber, the reaction rate of OH with cyclohexane is ~60 times greater than that with α-pinene. After the cyclohexane concentration had stabilized in the chamber for 30 min, a known concentration (~50 ppb in all experiments) of α-pinene (Sigma Aldrich, > 99 %) was injected into the chamber, followed by inorganic seed aerosol via atomization of an aqueous ammonium sulfate (AS) solution (in seeded experiments). To vary the seed aerosol surface area, different concentrations of AS solutions were used to generate seed aerosol particles in the seeded experiments. In the "low AS" experiments, a 0.015 M AS solution was used to generate seed particles, and the resulting initial total AS seed surface area concentration was ~1000 μm^2 cm^{-3}. In the "high AS" experiments, a 0.05 M AS solution was used to generate seed aerosol particles, and the resulting initial total AS seed surface area concentration was ~3000 μm^2 cm^{-3}. In selected experiments, no seed aerosol particles were introduced into the chamber and SOA was formed via nucleation. After the seed aerosol concentration in the chamber stabilized, O_3 (100 or 500 ppb), which was generated by passing purified air into a photochemical cell (Jelight 610), was introduced into the chamber. The start of O_3 injection into the chamber marked the beginning of the reaction (i.e., reaction time = 0 min). The injected α-pinene:O_3 molar ratio was approximately 1:2 and 1:10 in the 100 and 500 ppb O_3 experiments, respectively. O_3 was

injected into the chamber for 13.5 and 54.25 min in the 100 and 500 ppb O_3 experiments, respectively, to achieve the desired O_3 concentrations. Approximately 11 % and 98 % of the initial α-pinene had reacted when O_3 injection was completed in the 100 and 500 ppb O_3 experiments, respectively. In the GTEC chamber, α-pinene closest to the O_3 injection port likely reacted first in the α-pinene ozonolysis experiments. The O_3 injection times were established in separate experiments in which only O_3 was injected into the chamber. Based on the O_3 time series traces in the O_3-only experiments, the O_3 mixing timescale was estimated to be ~12 min for all experiments.

The α-pinene and O_3 concentrations were measured by a Gas Chromatograph-Flame Ionization Detector (GC-FID, Agilent 7890A) and O_3 monitor (Teledyne T400), respectively. GC-FID measurements were taken 12 min apart. A High Resolution Time-of-Flight Aerosol Mass Spectrometer (HR-ToF-AMS, Aerodyne Research Inc.) was used to measure the aerosol elemental composition (DeCarlo et al., 2006; Canagaratna et al., 2015). Details on the operation of the HR-ToF-AMS and its data analysis are described elsewhere (Canagaratna et al., 2015). Aerosol size distributions, number and volume concentrations were measured by a Scanning Mobility Particle Sizer (SMPS, TSI), which consists of a Differential Mobility Analyzer (DMA, TSI 3081) and a Condensation Particle Counter (CPC, TSI 3775). For nucleation and low AS experiments, the measured aerosol size range was set to 14 to 686 nm diameter. For high AS experiments, the measured aerosol size range was set to 17 to 983 nm. Prior checks were made to confirm that no particles larger than 686 nm were detected in the nucleation and low AS experiments. The SOA mass concentrations reported in this study were measured using the SMPS. The SOA density was calculated from the ratio of the aerosol size distributions measured by the HR-ToF-AMS and the SMPS during nucleation experiments (DeCarlo et al., 2004; Bahreini et al., 2005).

2.2. Particle wall deposition correction

Particle wall deposition needs to be accounted for to determine the SOA mass concentration in the chamber. Two limiting assumptions have traditionally been made regarding interactions between particles deposited on the chamber walls and suspended vapors when accounting for particle wall loss in the computation of SOA mass yields

(Weitkamp et al., 2007; Hildebrandt et al., 2009; Loza et al., 2012; Zhang et al., 2014). The first case assumes that particles deposited on the walls cease to interact with suspended vapors, and therefore the SOA mass present on these deposited particles does not change after deposition (Loza et al., 2012; Zhang et al., 2014). Adding the SOA mass present on these deposited particles to that present on the suspended particles provides a lower bound of the total SOA mass concentration. In the second case, it is assumed that particles deposited on the walls continue to interact with suspended vapors as if these particles had remained suspended, and therefore the SOA mass present on these deposited particles increases at the same rate as those suspended (Hildebrandt et al., 2009; Weitkamp et al., 2007). Thus, this case provides an upper bound of the total SOA mass concentration due to the additional uptake of suspended vapors to wall-deposited particles. However, it must be kept in mind that the calculated SOA mass concentration can be underestimated even in the upper bound case since the calculation accounts neither for differences in the vapor-particle and vapor-wall interaction and transport timescales nor for the significantly larger amount of absorbing mass of the chamber walls (relative to the deposited particles) for suspended vapors (McVay et al., 2014; Zhang et al., 2014; McVay et al., 2016).

In this study, we calculate SOA mass yields using the lower bound of the total SOA mass concentration obtained from SMPS measurements, which has been described in detail previously (Loza et al., 2012), and will be reviewed briefly here. For each particle size bin i at each time increment Δt, the particle number distribution deposited on the wall ($n_{w,i,j}$) is:

$$n_{w,i,j} = n_{s,i,j} \times (1 - \exp(-\beta_i \Delta t)) \quad (1)$$

where $n_{s,i,j}$ is the suspended particle number distribution in particle size bin i at time step j, Δt is the difference between time step j and time step $j + 1$, and β_i is the size-dependent first-order exponential wall loss rate obtained from seed-only experiments. As we describe subsequently, β_i may be measured directly during seed-only experiments or may be corrected for the influence of coagulation using a particle dynamics model. The

particle wall loss corrected number distribution ($n_{total,i,j}$) is obtained from the sum of the particle number distribution of deposited particles ($n_{w,i,j}$) and suspended particles ($n_{s,i,j}$):

$$n_{total,i,j} = n_{s,i,j} + n_{w,i,j} \quad (2)$$

Assuming spherical particles, the particle wall loss corrected volume concentration ($V_{total,j}$) is:

$$V_{total,j} = \sum_{i=1}^{m} \frac{n_{total,i,j}}{D_{p,i} \ln 10} \times (D_{p,i+} - D_{p,i-}) \times \frac{\pi}{6} D_{p,i}^3 \quad (3)$$

where m is the number of particle size bins, $D_{p,i+}$ and $D_{p,i-}$ are the upper and lower limits for size bin i, respectively, and $D_{p,i}$ is the median particle diameter for size bin i. The term $D_{p,i}$ln10 is needed to convert from a lognormal distribution. Figures S1-S4 and Table S1 show results from the particle wall loss correction. To calculate the SOA mass concentration ($\Delta M_{o,j}$), the SOA density (ρ_{org}) is multiplied by the difference of the particle wall loss corrected volume concentration ($V_{total,j}$) and the initial seed volume concentration (V_{seed}):

$$\Delta M_{o,j} = \rho_{org} \times (V_{total,j} - V_{seed}) \quad (4)$$

The measured densities of the α-pinene SOA are 1.39 and 1.37 g cm^{-3} for the 100 and 500 ppb O_3 experiments, respectively, and are within the range (i.e., 1.19 to 1.52 g cm^{-3}) reported in previous α-pinene ozonolysis studies (Bahreini et al., 2005; Kostenidou et al., 2007; Song et al., 2007; Shilling et al., 2009).

3. Vapor-particle dynamics model

A coupled vapor-particle dynamics model is used to evaluate the influence of seed aerosol surface area and oxidation rate on SOA formation in the α-pinene ozonolysis chamber experiments. This model is similar to that used in McVay et al. (2014), and will be briefly described here. Parameters from the experimental data (temperature, pressure, initial α-pinene concentration) are used as model inputs. The initial size distribution is set to that measured by the SMPS, with the exception of the two nucleation experiments. Because nucleation is not explicitly simulated, an approximation is used in which the

smallest diameter bin is initialized with the total number of particles measured at the end of the experiment (see Table S1). In each simulation, the decay of α-pinene, the consumption of O_3, the SOA mass concentration, and the SOA mass yield are calculated throughout the duration of the experiment. We assume a linear injection rate of O_3 based on the time required to inject the desired O_3 concentration. For example, O_3 is injected at a rate of 500/54.25 ppb min^{-1} for the first 54.25 min during the 500 ppb O_3 experiments. O_3 simultaneously decays by reaction with α-pinene at a rate constant of 9.4×10^{-17} cm^3 $molec.^{-1}$ s^{-1} (Saunders et al., 2003). Modeled O_3 and α-pinene concentrations are compared with observed concentrations in Fig. S5. The good fit of modeled and observed O_3 and α-pinene concentrations indicates that our representation of O_3 is appropriate. The O_3+α-pinene reaction is assumed to occur in a well-mixed chamber and produces 5 classes of first-generation products, which are grouped according to mass saturation concentrations, similar to the volatility basis set (Donahue et al., 2006): $>10^3$ (assumed to be completely volatile), 10^2, 10, 1 and 0.1 μg m^{-3}. Branching ratios between these products are optimized to fit the experimental data. These branching ratios cannot be compared directly to previously reported VBS parameters for α-pinene ozonolysis (e.g. Henry et al. (2012)) since VBS parameters are typically mass-based, while the branching ratios in the model are mole-based. Furthermore, the branching ratios here account for the influence of vapor wall deposition, while typical VBS parameters do not. We assume that these 5 classes of products have molecular weights 168, 184, 192, 200 and 216 g $mole^{-1}$ based on the group contribution method (Donahue et al., 2011). The first-generation products are assumed not to undergo further reaction with O_3 upon formation.

The aerosol dynamics in the chamber obey the aerosol general dynamic equation (Seinfeld and Pandis, 2006):

$$\left(\frac{\partial n(D_p,t)}{\partial t}\right) = \left(\frac{\partial n(D_p,t)}{\partial t}\right)_{\text{coag}} + \left(\frac{\partial n(D_p,t)}{\partial t}\right)_{\text{cond/evap}} + \left(\frac{\partial n(D_p,t)}{\partial t}\right)_{\text{wall loss}} \quad (5)$$

Coagulation is not considered in the present model; we address the potential impact of coagulation later in the paper. The change in particle number distribution due to particle wall loss is:

$$\left(\frac{\partial n(D_p,t)}{\partial t}\right)_{\text{wall loss}} = -\beta_j(D_p)n(D_p,t) \quad (6)$$

where, as noted in section 2.2, $\beta_j(D_p)$ is the size-dependent first-order wall loss rate coefficient obtained from fitting seed-only experiments. The rate at which vapor condenses onto a spherical aerosol particle is:

$$J_i = 2\pi D_p D_i (G_i - G_i^{eq}) F_{FS} \quad (7)$$

where G_i is the concentration of gas-phase species i, G_i^{eq} is the saturation concentration of gas-phase species i, D_i is the gas-phase molecular diffusivity (assumed to be 3×10^{-6} m^2 s^{-1} (McVay et al., 2014)), and F_{FS} is the Fuchs-Sutugin correction for non-continuum gas-phase diffusion:

$$F_{FS} = \frac{0.75\alpha_p(1+\text{Kn})}{\text{Kn}^2 + \text{Kn} + 0.283\text{Kn}\alpha_p + 0.75\alpha_p} \quad (8)$$

where α_p is the vapor-particle mass accommodation coefficient, and Kn is the Knudsen number, $\text{Kn} = 2\lambda_{AB}/D_p$. The vapor-particle mass accommodation coefficient accounts for any resistance to vapor molecule uptake at the particle surface (e.g. surface accommodation and particle-phase diffusion limitations). λ_{AB} is the mean free path of the gas-phase species, which is:

$$\lambda_{AB} = 3D_i \times \sqrt{\frac{\pi M_i}{8RT}} \quad (9)$$

where R is the ideal gas constant, T is the temperature, and M_i is the molecular weight of diffusing gas-phase molecule i. For each particle size bin, Eqs. 7-9 are used to compute the flux of each gas-phase species to and from an aerosol particle, scaled by the particle number concentration in the size bin. The net rate of change for each gas-phase species due to evaporation or condensation is obtained from the total flux summed over all the particle size bins.

G_i^{eq} varies for each particle size bin because it depends on the mass concentration of species *i* and the total organic mass concentration in the size bin:

$$G_i^{eq} = \frac{A_i C_i^*}{\sum_k A_k + M_{init}} \quad (10)$$

where A_i is the concentration of species *i* in the particle phase, C_i^* is the saturation concentration of species *i*, $\sum_k A_k$ is the sum of all the species concentration in the particle phase, and M_{init} is the mass concentration of any absorbing organic material initially present in the seed aerosol. To avoid numerical errors in Eq. 10 at the first time step, M_{init} is set to 0.01 μg m^{-3}.

The oxidation products of α-pinene ozonolysis are assumed to be subject to vapor-wall deposition, which is simulated using a first-order wall-loss coefficient (McMurry and Grosjean, 1985):

$$k_{wall,on} = \left(\frac{A}{V}\right) \frac{\frac{\alpha_{wall}\bar{c}}{4}}{1 + \frac{\pi}{2}\left(\frac{\alpha_{wall}\bar{c}}{4\sqrt{k_e D_i}}\right)} \quad (11)$$

where *A/V* is the surface area-to-volume ratio of the chamber (estimated to be 2.5 m^{-1}), α_{wall} is the vapor-wall mass accommodation coefficient, and k_e is the eddy diffusion coefficient that describes mixing conditions in the chamber. Based on the measured size-dependent particle wall loss rates (method is described in Zhang et al. (2014)), k_e is estimated to be 0.03 s^{-1} for the GTEC chamber. Vapor-wall deposition is assumed to be reversible, and the rate constant of vapor desorption from the chamber walls is:

$$k_{wall,off} = \frac{k_{wall,on}}{K_W C_W} = k_{wall,on}\left(\frac{C_i^* M_w \gamma_w}{C_W M_p \gamma_p}\right) \quad (12)$$

where C_w is the equivalent organic mass concentration in the wall (designated to treat gas-wall partitioning in terms of gas-particle partitioning theory and not necessarily

311 representative of a physical layer of organic concentration on the wall (Matsunaga and
312 Ziemann, 2010)), K_w is the gas-wall partitioning coefficient, M_w is the effective molecular
313 weight of the wall material, γ_w is the activity coefficient of the species in the wall layer,
314 M_p is the average molecular weight of organic species in the particle, and γ_p is the activity
315 coefficient of the species in the particle. For simplicity, we assume that $M_w = M_p$ and $\gamma_w =$
316 γ_p. C_w is set to 10 mg m^{-3} based on previous inferences by Matsunaga and Ziemann
317 (2010). Sensitivity studies (not shown) show no change in model predictions when
318 varying C_w above $C_w = 0.1$ mg m^{-3}.

319 In the initial version of the model, after all the α-pinene is consumed, vapor wall
320 deposition was assumed to continue to deplete the gas-phase oxidation products and
321 aerosol mass evaporates to maintain gas-particle equilibrium. SOA evaporation was not
322 observed experimentally (i.e., the SOA mass concentration does not decrease
323 significantly over time after peak SOA growth has been achieved in these chamber
324 experiments (Fig. 2)). In order to represent these observations in the model, a first-order,
325 particle-phase reaction is introduced by which aerosol species are converted into non-
326 volatile absorbing organic mass with a timescale of τ_{olig}. This mechanism (which is not
327 included in the model used in McVay et al. (2014)) is similar to that used by the
328 sequential equilibrium partitioning model, in which aerosol is converted from an
329 absorbing to non-absorbing, non-volatile phase in order to explain the inhibited diffusion
330 and evaporation observed in α-pinene ozonolysis SOA (Cappa and Wilson, 2011).
331 Although we assume here that the converted non-volatile aerosol mass still participates in
332 partitioning, either mechanism invokes a particle-phase process to retard SOA
333 evaporation.

334 In order to determine the parameters for α_w, α_p, τ_{olig} and the branching ratios
335 between the oxidation products that provide the best fit to measured SOA data, the
336 parameter space was discretized and all possible combinations of parameters were
337 simulated, following Karnezi et al. (2014). In order to restrict the number of
338 combinations required, only parameter values judged to be physically realistic were
339 chosen. Because the branching ratios in this model are mole-based, they must sum to one;
340 therefore only combinations of parameters summing to one were allowed. The

discretization is shown in Table S2 and results in roughly 10,000 different combinations of parameters. All six experiments were simulated with each parameter combination, and simulations were run using GNU Parallel (Tange 2011). For each combination of parameters, the percentage error was calculated from equation 10 of Karnezi et al. (2014):

$$E_i = \frac{100}{n}\sqrt{\sum_i^n (Moa_{i,guess} - Moa_{i,meas})^2} \quad (13)$$

where $Moa_{i,guess}$ is the model-predicted SOA mass concentration at a particular timestep i for one of the experiments, $Moa_{i,meas}$ is the measured SOA mass concentration at a particular timestep i for one of the experiments, and n is the number of timesteps summed over all experiments. The best-fit combination of parameters is defined as the combination of parameters with the lowest percentage error. This lowest-error combination of parameters was compared to the "best estimate" parameters determined from the inverse error weighting factor of Karnezi et al. (2014):

$$\bar{x} = \frac{\sum_j^N \left[x_j \frac{1}{E_j}\right]}{\sum_j^N \frac{1}{E_j}} \quad (14)$$

where x_j is a value of one of the parameters (α_w, α_p, τ_{olig} or a branching ratio between the oxidation products), with N different possible combinations of parameters, and E_j is the percent error for that particular combination of parameters. The lowest-error combination of parameters and the Karnezi et al. (2014) best estimate parameters are both reported, but the lowest-error combination of parameters resulted in a lower percentage error than the Karnezi et al. (2014) best estimate parameters. The lowest-error combination of parameters is used for the modeling analysis.

4. Results

Red and blue solid lines in Fig. 1 shows the size-dependent particle wall deposition coefficients measured in the low AS-seed only and high AS- seed-only deposition experiments. In these measurements, we assume that the number concentration is low enough such that the effect of coagulation is small and only particle wall

367 deposition affects the particle size distribution, thus allowing for the direct measurement
368 of size-dependent particle wall deposition coefficients. The initial total AS seed surface
369 area concentration in the low AS-seed only and high AS-seed only experiments (which
370 are conducted using 0.015 M AS and 0.05 M AS solutions, respectively) are similar to
371 those used in the α-pinene ozonolysis experiments (i.e., ~1000 and ~3000 $\mu m^2\ cm^{-3}$,
372 respectively). As shown in Fig. 1, the measured particle wall deposition coefficients from
373 the low AS-seed only and high AS-seed only experiments generally fall within the range
374 of those measured in routine monthly AS-seed only experiments conducted in the
375 chamber. Figure 1 also shows the size-dependent particle wall deposition coefficients
376 corrected for coagulation, shown using dashed lines, which are obtained as described in
377 Pierce et al., 2008 using the data from the low AS-seed only and high AS-seed only
378 experiments. A comprehensive description of the relationship between coagulation and
379 particle wall deposition will be provided in a forthcoming publication. Briefly, as
380 described in Pierce et al. (2008), the coagulation-corrected particle wall loss coefficients
381 are determined by simulating the decay of the initial size distribution due to coagulation
382 and then attributing the difference in this decay and the observed decay to particle wall
383 loss. For both the measured and coagulation-corrected particle wall deposition
384 coefficients, the minimum coefficient for the low AS-seed only experiment is different
385 from that of the high AS-seed only experiments. The cause of this difference is currently
386 under investigation but may be due in part to uncertainties arising from the low particle
387 number concentrations for the larger particles in the low AS-seed only experiment. To
388 study how coagulation can potentially affect SOA mass yields in this study, both the
389 measured and coagulation-corrected size-dependent particle wall deposition coefficients
390 are used to correct for particle wall deposition in the α-pinene ozonolysis experiments.

391 Assuming that the effect of coagulation is small, the particle wall deposition
392 corrected number concentration data provide a test of the appropriateness of the particle
393 wall deposition correction. The corrected number concentration should level off at a
394 constant value (i.e., the initial particle number concentration), assuming no significant
395 coagulation, when particle wall deposition is properly accounted for since the wall-
396 deposited particle number distribution is added to the suspended particle number
397 distribution during particle wall loss correction. Neglecting coagulation, we account for

particle wall deposition in nucleation and low AS experiments using deposition coefficients measured from the low AS-seed only experiments, while particle deposition in high AS experiments are accounted for using coefficients measured from the high AS-seed only experiments. Figures S1 and S2 show the particle wall deposition-corrected aerosol number and volume concentrations. Over all experiments, the particle wall deposition-corrected final particle number concentration (i.e., at the end of the reaction) is 9 to 17 % less than the initial particle number concentration for the low AS and high AS experiments (Table S1), respectively, indicating that the particle wall deposition-corrected volume concentrations are slightly underestimated. The fact that the particle wall deposition-corrected final particle number concentrations are somewhat smaller than the initial particle number concentrations may be due to variations in particle wall deposition rates in the AS-seed only and α-pinene ozonolysis experiments or to coagulation. To first examine variations in particle wall deposition rates, we used the average of the measured low AS-seed only and high AS-seed only particle wall deposition coefficients to account for particle wall deposition in all the experiments (Figs. S3 and S4). While there is a negligible difference in the particle wall deposition corrected volume concentrations (Figs. S3 and S4 vs. Figs. S1 and S2), a larger spread (1 to 22 %) exists in the difference between the initial and final particle number concentrations when the average measured particle wall deposition coefficients are used (Table S1). Therefore, all subsequent nucleation and low AS data presented here are particle wall deposition-corrected using coefficients measured from the low AS-seed only experiments, and all high AS data are corrected using particle wall deposition coefficients measured from the high AS-seed only experiments. We furthermore conclude that variations in particle wall deposition rates do not cause the decrease in the particle wall deposition-corrected final number concentration and is most likely due to coagulation. Thus, the SOA data are also corrected using the coagulation-corrected particle wall deposition coefficients (discussed below). We show subsequently the relatively minor difference that correcting for coagulation has on overall SOA mass yields. Therefore, we use SOA concentrations corrected using the measured particle wall deposition coefficients for the bulk of the analysis in this study.

Figure 2 shows the reaction profiles of the α-pinene ozonolysis experiments. SOA growth typically starts within 10 to 20 min of the start of the reaction. At either O_3 concentration, the molar ratio of O_3 reacted to α-pinene reacted is approximately 1:1 (i.e., 50 ppb α-pinene reacted with 50 ppb O_3), which indicates that O_3 reacts only with α-pinene and not its oxidation products. As anticipated, the α-pinene oxidation rates in the 100 ppb O_3 experiments are significantly slower than those in the 500 ppb O_3 experiments. Figures 2a-c show that peak SOA levels are typically reached at reaction time ~300 to 350 min in the 100 ppb O_3 experiments, during which ≥ 95 % of the injected α-pinene has reacted. In contrast, all the α-pinene reacts within 80 to 90 min of the start of reaction in the 500 ppb O_3 experiments, and peak SOA levels are achieved at reaction time ~100 min (Figs. 2d-f). These results indicate that the O_3 concentration dictates both the rate of α-pinene oxidation and the time it takes to achieve peak SOA growth.

Figure 3 shows the time-dependent growth curves (SOA mass concentration vs. α-pinene reacted (Ng et al., 2006)) for the 100 and 500 ppb O_3 experiments. Only SOA growth data up to SOA peak concentrations are shown. SOA growth essentially stops once all the α-pinene has reacted. This is expected, as α-pinene has only one double bond; the first step of α-pinene ozonolysis is rate-limiting and the first-generation products are condensable (Ng et al., 2006; Chan et al., 2007). The time-dependent SOA growth curves for experiments corresponding to different seed aerosol concentrations overlap for both low and high O_3 concentrations. This indicates that the initial AS seed surface area does not influence the SOA growth rate within the range of AS seed surface area concentration used. It is important to note that while it appears that the SOA growth rate is faster in the 100 ppb O_3 relative to the 500 ppb O_3 experiments based on the time-dependent growth curves shown in Fig. 3, this is not the case. Instead, the observed time-dependent growth curves can be explained by the higher concentration of α-pinene having reacted during the 10 to 20 min delay of SOA formation in the 500 ppb O_3 experiments compared to the 100 ppb O_3 experiments (Fig. 2).

Figure 4 shows the time-dependent SOA mass yields as a function of initial total AS seed surface area for the 100 and 500 ppb O_3 experiments. Regardless of the O_3

concentration, the SOA mass yields stay roughly constant despite the increase in AS seed surface area. This indicates that the surface area concentration of AS seed aerosol does not noticeably influence the partitioning of gas-phase α-pinene ozonolysis products to the particle phase within the range of AS seed surface area concentration used. Higher SOA mass yields are observed in the 500 ppb O_3 experiments, which indicates that the α-pinene oxidation rate controls the absolute amount of SOA formed. It is important to note that these conclusions are robust even when the average of the measured low AS-seed only and high AS-seed only particle wall loss coefficients are used to account for particle wall loss in all the experiments (Fig. S6). The enhancement of SOA mass yields at higher O_3 concentrations and the lack of a SOA mass yield dependence on AS seed surface area (within the range of AS seed surface area concentration used in this study) will be discussed further in Section 5.

The α-pinene ozonolysis SOA mass yields obtained in this study are compared to those reported in previous studies in Fig. 5. Table S3 lists the experimental conditions employed in these studies. To facilitate comparison between the different studies, all the SOA mass yield and concentration data (including this study) are adjusted to an organic density of 1.0 g cm^{-3}. As shown in Fig. 5, the SOA mass yields obtained at peak SOA growth in this study are generally consistent with those of previous studies where the chamber was operated in batch mode (that in this study).

To investigate the influence of coagulation on the SOA mass yields, the coagulation-corrected size-dependent particle wall deposition coefficients are also used to correct for particle wall deposition in the α-pinene ozonolysis experiments. Specifically, all nucleation and low AS data are particle wall deposition-corrected using coagulation-corrected coefficients derived from the low AS-seed only experiments, and all high AS data are corrected using coagulation-corrected particle wall deposition coefficients derived from the high AS-seed only experiments. Figure S7 shows the time-dependent SOA mass yields (obtained using the coagulation-corrected and measured particle wall deposition coefficients) as a function of initial total AS seed surface area. SOA mass yields obtained using the coagulation-corrected particle wall deposition coefficients are < 2 % (absolute values) higher than those using the measured particle wall deposition

coefficients. Similar to the SOA mass yields obtained using the measured particle wall deposition coefficients (Figs. 4, S7c and S7d), SOA mass yields obtained using the coagulation-corrected particle wall deposition coefficients stay roughly constant despite the increase in AS seed surface area for both O_3 concentrations, and the SOA mass yields are higher in the 500 ppb O_3 experiments (Figs. S7a and S7b). The mass yields obtained at peak SOA growth are also generally consistent with those of previous studies (Fig. S8). Taken together, this suggests that the effect of coagulation on the SOA mass yields is likely minor for the aerosol concentrations used in this study. Therefore, only data that have been particle wall deposition-corrected using coefficients measured in the low AS-seed only and high AS-seed only experiments are fitted to determine model parameters for the vapor-particle dynamics model described in Section 3.

As noted earlier, optimal model values for α_p, α_w, τ_{olig} and the branching ratios between the oxidation products were determined by calculating the error between the observed and modeled time-dependent SOA concentrations for all possible combinations of model parameters. The combination of parameters with the lowest percent error is $\alpha_w = 10^{-6}$, $\alpha_p = 0.1$, $\tau_{olig} = 4$ h, branching ratios = 0.6, 0.3, 0.05, 0.05 and 0 for oxidation products with vapor pressures $>10^3$, 10^2, 10, 1 and 0.1 μg m^{-3}, respectively. This combination of parameters results in a percent error of 21% (Table S4). It is important to note that predictions using $\alpha_p = 0.1$ or 1 resulted in very similar errors; with the same combination of parameters and $\alpha_p = 1$, the percent error only increased to 22%. The "best estimate" parameters determined following the Karnezi et al. (2014) method are as follows: $\alpha_w = 3.6\times10^{-6}$, $\alpha_p = 0.35$, $\tau_{olig} = 6$ h, and branching ratios = 0.66, 0.16, 0.06, 0.06, and 0.06 for oxidation products with vapor pressures $>10^3$, 10^2, 10, 1 and 0.1 μg m^{-3}, respectively. This combination of parameters results in an error of 37% (Table S4). Model predictions using both sets of parameters are compared to measured SOA concentrations in Fig. S9. The lowest-error parameters are used for the analysis in the remainder of this study. The best-fit $\alpha_w = 10^{-6}$ corresponds to a first-order vapor-wall deposition rate constant ($k_{wall,on}$) of 10^{-4} s^{-1}. A wide range of vapor wall loss rates has been reported (Figure 3 of Krechmer et al. (2016)). This $k_{wall,on}$ value is comparable to that reported by Matsunaga and Ziemann (2010) for a 8.2 m^3 chamber but significantly faster than wall loss rates that have been measured in the Caltech chamber (Zhang et al.,

519 2015). The reason for this wide range of reported vapor wall loss rates is currently
520 uncertain and outside the scope of this study.

521 **5. Discussion**

522 α-pinene ozonolysis has been carried out at two O_3 mixing ratios (100 and 500
523 ppb) under varying AS seed aerosol surface area concentrations (0, ~1000 and ~3000 μm^2
524 cm^{-3}).

525 **5.1 Seed aerosol surface area effect**

526 Figure 3 shows that the time-dependent SOA growth curves for experiments with
527 different seed area concentrations overlap at both O_3 concentrations, which indicates the
528 AS seed surface area does not affect the rate of SOA growth within the range of AS seed
529 surface area concentration used in this study. This observation differs from findings by
530 Pathak et al. (2007b) for the O_3+α-pinene system, who showed that even though the final
531 SOA mass yields measured in the reaction of 7.3 ppb α-pinene with 1500 ppb O_3 were
532 similar in their seeded and unseeded experiments, SOA growth was considerably slower
533 in unseeded experiments compared to seeded experiments. The authors suggested that the
534 slow SOA formation rate in their unseeded experiment was the result of SOA formation
535 being limited by the mass transfer of semi-volatile oxidation products to newly formed
536 particles (via nucleation) during the early stages of the experiment. These newly formed
537 particles have a significantly smaller aerosol surface area for gas-particle partitioning as
538 compared to that of seed aerosol particles in the seeded experiments. Consequently, the
539 semi-volatile oxidation products accumulated in the gas phase during the early stages of
540 the unseeded experiments, resulting in slower SOA growth compared to the seeded
541 experiments. The observation that the presence of seed aerosol does not influence the
542 SOA growth rate in the present study may be explained by the relatively high
543 concentrations of α-pinene reacted and SOA mass loadings obtained. Previous studies
544 have shown that the delay between the onset of VOC oxidation and SOA formation in
545 unseeded experiments is most pronounced at low aerosol loadings (Kroll et al., 2007).
546 We note that the concentrations of α-pinene reacted and SOA mass loadings obtained in
547 this study are significantly larger than those reported by Pathak et al. (2007b). Therefore,

548 it is possible that due to the relatively large concentrations of α-pinene reacted in this
549 study, substantial concentrations of gas-phase oxidation products are generated, which
550 results in rapid partitioning into the particle phase even in the absence of seed aerosol.
551 This is evident from the large increase in the particle number concentration during the
552 early stages of the unseeded 100 and 500 ppb O_3 experiments, where the particle number
553 concentration increased to ~8000 and ~10000 particles/cm^3 during the first 45 min of the
554 100 and 500 ppb O_3 experiments, respectively (Fig. S1a and S2a). Thus, the SOA growth
555 rates are not controlled by the presence of AS seed in this study.

556 Figure 4 shows that for both O_3 mixing ratios used, the time-dependent SOA mass
557 yield is similar at any given AS seed surface area (see also Table 1). The absence of a
558 SOA growth dependence on the AS seed surface area is similar to observations reported
559 by McVay et al. (2016) for the α-pinene photooxidation (OH-driven chemistry) system,
560 but differ from those reported by Zhang et al. (2014) for the toluene photooxidation
561 system in which the SOA mass yield increased with the surface area concentration of
562 seed aerosol.

563 The best-fit $\alpha_p = 0.1$ (or $\alpha_p = 1$, with almost the same percentage error) suggests
564 the absence of significant limitations to vapor-particle mass transfer in the present α-
565 pinene ozonolysis study, and that SOA formation is governed by quasi-equilibrium
566 growth (Saleh et al., 2013; McVay et al., 2014), which occurs when SOA-forming vapors
567 are produced at a rate that is significantly slower than that required to establish gas-
568 particle equilibrium (Shiraiwa and Seinfeld, 2012; Zhang et al., 2012). Moreover, the
569 characteristic timescale to establish gas-particle equilibrium is less than those for reaction
570 and vapor-wall deposition. When the vapor and particle phases maintain equilibrium,
571 gas-particle equilibrium is controlled by the amount of organic matter in the VOC
572 system. As a result, the rate of condensation of SOA-forming vapors is independent of
573 the seed aerosol surface area (McVay et al., 2014). The best-fit $\alpha_p = 0.1$ is within the
574 range of α_p coefficients determined from α-pinene ozonolysis SOA thermodenuder
575 studies ($\alpha_p = 0.1$) (Saleh et al., 2013; Saha et al., 2016) and α-pinene photooxidation
576 chamber studies ($\alpha_p = 0.1$ or 1) (McVay et al., 2016). Notably, this result differs markedly
577 from that for toluene photooxidation (Zhang et al., 2014), where α_p was determined to be

0.001, and for which, since the SOA mass yield was strongly dependent on the seed aerosol surface area, the condensation of SOA-forming vapors onto seed aerosol particles was kinetically limited (McVay et al., 2014). Kinetically-limited SOA growth occurs when the timescale for gas-particle equilibrium is competitive with or exceeds the timescale for reaction and vapor wall deposition, and may reflect imperfect accommodation of gas-phase organics to the particle phase. The markedly different behavior of the α-pinene and toluene SOA systems could be due to differences in SOA volatility and aerosol physical phase state (McVay et al., 2016).

5.2 Oxidation rate effect

At higher O_3 concentrations, the α-pinene oxidation rate increases, leading to higher SOA mass yields (the "oxidation rate effect"). This behavior was previously observed by Ng et al. (2007) for the *m*-xylene photooxidation system, for which the oxidation rate effect was attributed to the loss of semi-volatile condensable products to chamber walls in competition with condensation onto seed particles to form SOA.

SOA formation from α-pinene ozonolysis is presumed to be driven by a range of semi- and low-volatility first-generation products arising from reaction of O_3 with the single C=C double bond (Ng et al., 2006). These products are subject to two competing routes: condensation to particles to form SOA or deposition on the chamber walls. Each process can be represented in terms of a first-order rate constant: $k_{wall,on}$ and $k_{particle,on}$ (s^{-1}). The rate of vapor-wall deposition of condensable species A is then $k_{wall,on}$ × [A] (molec cm^{-3} s^{-1}) and the rate of condensation onto particles is $k_{particle,on}$ × [A] (molec cm^{-3} s^{-1}). Increasing the rate of reaction increases the concentration of [A], but the relative rates of vapor-wall deposition and condensation onto particles will remain the same. In general, however, both vapor-wall deposition and vapor-particle condensation are reversible processes (McVay et al., 2014; Zhang et al., 2014). The first-order rate constant for evaporation from the wall can be represented as (Matsunaga and Ziemann, 2010):

$$k_{wall,off} = k_{wall,on}\left(\frac{C_i^*}{C_w}\right) \quad (15)$$

where C_i^* is the saturation concentration and C_w is the assumed equivalent wall organic concentration. The rate of evaporation from particles is:

$$k_{particle,off} = k_{particle,on}(\frac{C_i^*}{C_{aer}}) \quad (16)$$

where C_{aer} is the organic aerosol concentration ($C_{aer}=\sum A_k+M_{init}$).

The difference between C_{aer} and C_w is the key to explaining the oxidation rate effect. At the beginning of the experiment, C_{aer} is very small because the inorganic seeds are essentially non-absorbing. Therefore, $k_{particle,off}$ is large, and the net SOA growth is small. In contrast, C_w is considered to be substantial (on the order of 10 mg m^{-3}) and to be essentially constant throughout the experiment (Matsunaga and Ziemann, 2010; McVay et al., 2014; Zhang et al., 2014). Model predictions are insensitive to the value of C_w since, in any event, C_w is significantly larger than C_{aer} (Zhang et al., 2014). Therefore, $k_{wall,off}$ is small at the beginning of the experiment and the net vapor wall loss rate is fast. As C_{aer} increases, the net SOA condensation rate increases relative to the net vapor wall loss rate. When the reaction rate increases corresponding to higher O_3 concentrations, C_{aer} grows more quickly because more condensable species are available to form SOA, and the net condensation rate increases more rapidly. Therefore, the observed oxidation rate effect is due to vapor wall deposition, and arises because vapor-particle and vapor-wall condensation are essentially reversible processes. This explanation is consistent with simulations varying the O_3 concentration in which all species are non-volatile (i.e., do not evaporate from the particles or the wall). In this case, no oxidation rate effect is observed as the O_3 concentration increases. The growth curves for different O_3 concentrations overlap, and the same yield is obtained regardless of O_3 concentration (Fig. S10).

Sensitivity tests were performed to determine the point at which SOA formation is no longer influenced by the O_3 concentration. In these simulations, the initial α-pinene concentration is fixed at 48 ppb, while the O_3 concentration is varied from 75 to 1000 ppb. The rate of O_3 injection is assumed to remain constant as the O_3 concentration is increased to mimic the experimental protocol (i.e., O_3 injection time is increased to achieve higher O_3 concentrations). The O_3 injection rate used in these simulations is fixed

633 at 500/54.25 ppb min^{-1}, which is the same as that used to analyze results from the 500
634 ppb O_3 experiments. Model predictions in Fig. S11 show that the maximum SOA mass
635 concentration increases with increasing O_3 concentration up to approximately 500 ppb
636 O_3. Beyond this O_3 concentration, the SOA growth curves overlap and the maximum
637 SOA mass concentration does not increase even when more O_3 is added. This plateau
638 arises due to the lengthening time required to inject increasing amounts of O_3. More than
639 1 h is required to inject > 500 ppb of O_3, and by this time, virtually all of the α-pinene has
640 reacted. Increasing the O_3 concentration after all of the α-pinene has reacted does not lead
641 to any changes in the SOA mass concentration. However, if a faster injection rate of O_3 is
642 used, the oxidation rate effect will persist to higher O_3 concentrations (i.e., > 500 ppb O_3)
643 (Fig S12). With a faster injection rate, 500 ppb O_3 is injected before all of the α-pinene
644 has reacted. Continuing to inject O_3 to a higher concentration (i.e., 750 ppb) will cause α-
645 pinene to decay faster and SOA to grow faster than when the O_3 injection stops at 500
646 ppb. The oxidation rate effect is then apparent at higher O_3 concentrations. If, instead of
647 using an injection rate of O_3, simulations are run using fixed initial O_3 (not possible
648 experimentally), the rate effect persists to even higher O_3 concentrations. The relative
649 increase in yield with increasing O_3 concentrations slows at very high O_3 concentrations
650 because the rate of reaction becomes substantially faster than the vapor wall deposition
651 rate, and there is less marginal effect to increasing the reaction rate.

652 It should be noted that while we showed that the observed oxidation rate effect
653 (i.e., higher SOA mass yields as a result of faster hydrocarbon oxidation rates) is a
654 consequence of vapor-wall deposition, the possibility that differing peroxy radical (RO_2)
655 chemistry in the 100 and 500 ppb O_3 experiments may play some role in influencing the
656 SOA mass yields cannot be discounted. RO_2 radicals, which are formed from the
657 decomposition of excited Criegee intermediates (Docherty et al., 2005), may be produced
658 at faster rates in the 500 ppb O_3 experiments. This may lead to the higher production of
659 condensable oxidation products from the RO_2+RO_2 reaction pathway in the 500 ppb O_3
660 experiments (relative to those formed in the 100 ppb O_3 experiments), which may result
661 in higher SOA mass yields.

662 **5.3 Interplay of the seed aerosol surface area effect and the oxidation rate effect**

In this study, we observe an oxidation rate effect but not a seed aerosol surface area effect. In Zhang et al. (2014), a seed aerosol surface area effect was observed, but the variation of the oxidation rate was not studied. A key aspect of vapor wall deposition is the potential interplay between the seed aerosol surface area effect and the oxidation rate effect. To examine this interplay in the α-pinene ozonolysis system, simulations were carried out by varying the seed aerosol surface area and the O_3 concentration simultaneously, while using the branching ratios, oligomerization rate, and vapor wall deposition rate parameters obtained in the present study. The initial α-pinene concentration was set to 50 ppb, and a fixed O_3 concentration was used in place of a linear injection. α_p was varied at 0.001, 0.01, 0.1, and 1 in these simulations. Figure 6 shows the SOA mass yield at peak SOA growth as a function of both the seed aerosol surface area and O_3 concentration for α_p = 1, 0.1, 0.01, and 0.001. For α_p = 1 or 0.1, the oxidation rate dominates: SOA mass yield increases significantly as O_3 concentration increases while the seed aerosol surface area has a negligible effect. For α_p = 0.01, both effects can be observed in different regions: at low O_3 concentrations and high seed aerosol surface areas, the oxidation rate effect dominates; at low seed aerosol surface areas and high O_3 concentrations, the seed surface area dominates. At low seed aerosol surface areas and low O_3 concentrations, both effects are present. For α_p = 0.001, the seed aerosol surface area effect dominates except at very high seed aerosol surface areas. These observations show that the presence of an oxidation rate effect and/or seed aerosol surface area effect depends on a complex interplay of factors, such as α_p, the rate of hydrocarbon oxidation, and the amount of seed surface area present.

6. Implications

In this study, we systematically examine the roles of gas-particle partitioning and VOC oxidation rate in the presence of vapor-wall deposition in α-pinene ozonolysis. We show that despite the presence of vapor-wall deposition, SOA mass yields at peak SOA growth remain approximately constant regardless of the seed aerosol surface area (within the range of AS seed surface area concentration used in this study). This observation is consistent with SOA formation in the α-pinene ozonolysis system being governed by quasi-equilibrium growth, for which there are no substantial limitations to vapor-particle

mass transfer. This result was demonstrated in a previous modeling study which showed that increasing the seed-to-chamber surface area ratio will lead to increased SOA growth only in cases in which the condensation of SOA-forming vapors onto seed aerosol particles is kinetically limited as a result of imperfect accommodation of gas-phase organics to the particle phase (McVay et al., 2014).

An important implication of this study is that diverting vapor-wall deposition in chamber studies via the addition of ever-increasing quantities of seed aerosol particles is not effective in VOC systems for which SOA formation is governed by quasi-equilibrium growth. This study also underscores the importance of accounting for particle wall deposition appropriately in chamber studies, to avoid erroneous conclusions regarding the role of gas-particle partitioning (quasi-equilibrium vs. kinetically-limited SOA growth) in influencing vapor wall loss in the VOC system.

We note that the present study shows that the SOA mass yield is independent of seed aerosol surface area concentration for values ranging from 0 to ~3000 $\mu m^2\ cm^{-3}$. This corresponds to a seed-to-chamber surface area ratio of 0 to $\sim 1 \times 10^{-3}$, which is substantially smaller than the range used by Zhang et al. (2014) to study the influence of vapor-wall deposition on toluene photooxidation SOA formation in the Caltech chamber (i.e., 0 to $\sim 5 \times 10^{-3}$). It is possible that a SOA mass yield dependence on the seed surface area may have become more apparent had a larger range of seed aerosol surface area (i.e., $> 3000\ \mu m^2\ cm^{-3}$), and hence a larger range of seed-to-chamber surface area ratio, been used here. One consideration is that coagulation may become increasingly important, and will need to be accounted for, when higher seed aerosol number concentrations (relative to those used in this study) are used (Seinfeld and Pandis, 2006; Pierce et al., 2008). A detailed analysis of the effect of seed aerosol surface area concentrations $> 3000\ \mu m^2\ cm^{-3}$ on α-pinene ozonolysis SOA mass yields will be the subject of forthcoming work.

Higher SOA mass yields at peak SOA growth are observed in the present study when O_3 is increased from 100 to 500 ppb. This is because α-pinene is oxidized more quickly, which leads to gas-phase oxidation products being formed more rapidly, and consequently partitioning more quickly onto AS seed aerosol particles before they are lost to the chamber walls. Therefore, the oxidation rate effect (i.e., higher SOA mass

yields as a result of faster hydrocarbon oxidation rates) is a consequence of vapor-wall deposition. An important implication of this study is that SOA mass yields can be affected by vapor-wall deposition in VOC systems that are not characterized by slow mass accommodation of gas-phase organics to the particle phase (Zhang et al., 2014). Thus, this work demonstrates that the effect of vapor-wall deposition on SOA mass yields can be mitigated through the use of excess oxidant concentrations. It should be noted that the α-pinene ozonolysis SOA mass yields (absolute values) increased by 5 to 9 % when O_3 is increased from 100 to 500 ppb (for an initial α-pinene concentration of ~50 ppb), where SOA formation is governed by quasi-equilibrium growth. In the absence of vapor-wall deposition, SOA mass yields are predicted by the model used here to approximately double from those observed experimentally. In contrast, Zhang et al. (2014) showed that the presence of vapor-wall deposition led to underestimation of SOA formation by factors as much as four in the toluene photooxidation system, where the condensation of SOA-forming vapors onto seed aerosol is kinetically limited. Taken together, these results indicate that the magnitude by which vapor-wall deposition affects SOA mass yields depends on the extent to which the VOC system is governed by kinetically-limited SOA condensational growth.

Given these observations of how gas-particle partitioning can influence the magnitude by which vapor-wall deposition affects SOA mass yields, an overriding question is: what controls the gas-particle partitioning behavior of SOA formed in different VOC systems? α_p describes the overall mass transfer of vapor molecules into the particle phase (McVay et al., 2014; Zhang et al., 2014). Thus, α_p affects the vapor-particle equilibrium timescale, which, depending on the extent to which it is competitive with the timescales for reaction and vapor-wall deposition, determines whether SOA formation is governed by kinetically-limited or quasi-equilibrium growth. Markedly different α_p values could arise from the physical phase state of the SOA formed. As discussed by McVay et al. (2014, 2016), if the SOA formed exists in a semi-solid state (Vaden et al., 2010; Virtanen et al., 2010; Cappa and Wilson, 2011; Vaden et al., 2011; Virtanen et al., 2011; Kuwata and Martin, 2012; Perraud et al., 2012; Saukko et al., 2012; Abramson et al., 2013; Renbaum-Wolff et al., 2013), a low value of α_p might be expected owing to retarded surface accommodation and particle-phase diffusion (Zaveri et al.,

754 2014). Quantification of α_p is challenging experimentally, and reported α_p values for the
755 same system can vary by several orders of magnitude (Grieshop et al., 2007; Stanier et
756 al., 2007; Vaden et al., 2011; Miles et al., 2012; Saleh et al., 2013 Saha et al., 2016).
757 Therefore, α_p of SOA formed in different VOC systems need to be better constrained
758 through a combination of experimental and modeling efforts.

759 While not investigated in detail in this study, the timescale of oligomerization
760 may play an important role depending on the SOA growth regime (i.e., kinetically-
761 limited vs. quasi-equilibrium). Currently, it is unclear how the timescale of
762 oligomerization in a VOC system where SOA formation is dominated by quasi-
763 equilibrium growth (e.g. α-pinene ozonolysis) may differ from one that is dominated by
764 kinetically-limited growth (e.g. toluene photooxidation (Zhang et al., 2014)). This
765 requires further investigation through a combination of experimental and modeling
766 efforts to improve our understanding of how particle-phase processes (e.g.
767 oligomerization) affect gas-particle partitioning, and consequently influence the
768 magnitude by which vapor-wall deposition affects SOA mass yields.

769 The SOA mass yield from the ozonolysis of monoterpenes in the GEOS-CHEM
770 chemical transport model (19 % at 10 μg m^{-3}) is currently based on that measured in α-
771 pinene ozonolysis studies by Shilling et al. (2008) (Pye et al., 2010). Shilling et al. (2008)
772 measured these SOA mass yields in a teflon chamber operated in continuous-flow mode,
773 as opposed to batch mode, which is how experiments in the present study and most of
774 those shown in Fig. 5 and Table S3 were conducted. While it is not possible to directly
775 compare our results with those of Shilling et al. (2008) due to differences in SOA mass
776 concentrations, the SOA mass concentrations and yields measured in the current study
777 are generally consistent with those of previous batch chamber studies. The SOA mass
778 yields at ~10 μg m^{-3} SOA mass concentration measured by Shilling et al. (2008) are
779 generally higher than those measured in chambers operated in batch mode (Griffin et al.,
780 1999; Cocker et al., 2001b; Presto et al., 2005; Presto and Donahue, 2006; Pathak et al.,
781 2007b) (Fig. 5). One possible explanation for the higher SOA mass yields in the
782 continuous-flow, steady state, mode is that the SOA-forming vapors are in equilibrium
783 with the chamber walls and seed aerosol, hence minimizing the irreversible loss of SOA-

784 forming vapors to the chamber walls (Shilling et al., 2008). However, the extent to which
785 SOA mass yields obtained in a continuous-flow reactor are influenced by vapor wall loss
786 is unclear. Using a continuous-flow reactor, Ehn et al. (2014) observed α-pinene
787 ozonolysis SOA mass yields to increase with increasing seed aerosol surface area but
788 required $\alpha_p = 1$ to fit the observed SOA growth. The observed vapor-wall deposition rate
789 constant in their continuous-flow reactor (0.011 s^{-1}) is two orders of magnitude larger
790 than that of the GTEC chamber (10^{-4} s^{-1}). The estimated timescales for gas-particle and
791 gas-wall partitioning are also approximately equal in their continuous-flow reactor. This
792 indicates that SOA condensational growth is kinetically limited in their continuous-flow
793 reactor even at $\alpha_p = 1$ (Ehn et al., 2014; McVay et al., 2014), which suggests that SOA
794 mass yields measured in their continuous-flow reactor may be significantly affected by
795 vapor-wall deposition.

796 Previous studies on SOA formation from the OH and NO_3 oxidation of biogenic
797 VOCs have similarly reported higher SOA mass yields in the presence of higher oxidant
798 concentrations. For example, in the NO_3 oxidation of β-pinene, Boyd et al. (2015)
799 reported SOA mass yields 10 to 30 % higher than those previously reported by Fry et al.
800 (2009, 2014). In addition to differences in the experimental conditions of the two studies
801 (which may lead to differing RO_2 chemistry), Boyd et al. (2015) hypothesized that the
802 higher SOA mass yields could also be a result of the higher NO_3 concentrations used in
803 their study (which led to faster β-pinene oxidation rates) compared to those used by Fry
804 et al. (2009, 2014). The oxidation rate effect was also observed in the *m*-xylene
805 photooxidation system, where Ng et al. (2007) showed that the SOA mass yields were
806 dependent on the *m*-xylene oxidation rate, with higher OH concentrations (and hence
807 faster oxidation rates) resulting in higher SOA mass yields. The authors dismissed the
808 possibility of the different SOA mass yields being a result of different RO_2 chemistry
809 since all their *m*-xylene photooxidation experiments were performed under high-NO_x
810 conditions and the RO_2 reacted virtually entirely with NO. Together, these studies show
811 that faster hydrocarbon oxidation rates can alleviate the effects of vapor-wall deposition
812 on SOA mass yields in different VOC systems.

This gives rise to the question: should chamber SOA experiments on different VOC systems be performed under as rapid oxidation conditions as possible (i.e., large oxidant concentrations) to reduce the effects of vapor-wall deposition? A recent study by McVay et al. (2016) reported similar SOA growth under low and high OH levels for α-pinene photooxidation. The authors hypothesized that the autoxidation mechanism likely becomes a more important pathway at low OH levels (Crounse et al., 2013), and thus contributes substantially to SOA growth. Therefore, it is possible that certain reaction pathways and mechanisms (which are important in the atmosphere) are biased when unusually high levels of oxidants are used in chamber experiments (e.g. autoxidation). Thus, this underscores the need to design chamber experiments that simultaneously mitigate the magnitude of vapor-wall deposition while ensuring that reaction conditions, and consequently reaction pathways and oxidation products, are atmospherically relevant. More importantly, the impact of vapor-wall deposition on SOA formation and evolution in various VOC systems conducted under different reaction conditions (regardless of atmospheric relevance) needs to be quantified through a combination of experimental and modeling efforts. Similar to this study, experiments should be performed using different seed aerosol surface area and oxidant concentrations to study their influence on vapor-wall deposition and SOA mass yields. If the effects of vapor-wall loss are found to be strongly dependent on seed aerosol surface area and/or oxidant concentrations (e.g. toluene photooxidation, where SOA formation may be underestimated by factors as much as four (Zhang et al., 2014)), further experiments aimed at measuring the wall deposition rates of the oxidation products should be performed. These wall deposition rates can then be used in predictive models to determine the vapor-wall and vapor-particle mass accommodation coefficients of these oxidation products. Consequently, this will allow us to determine the fraction of SOA-forming vapors partitioning to the particle phase vs. lost to the chamber walls (Zhang et al., 2015; Krechmer et al., 2016).

Acknowledgements

This research was funded by NSF Grants 1455588 and AGS-1523500, and US Environmental Protection Agency STAR grant (Early Career) RD-83540301. This publication's contents are solely the responsibility of the grantee and do not necessarily

represent the official views of the US EPA. Further, US EPA does not endorse the purchase of any commercial products or services mentioned in the publication. R.C. McVay was supported by a National Science Foundation Graduate Research Fellowship under Grant No. DGE-1144469.

References

Abramson, E., Imre, D., Beranek, J., Wilson, J., and Zelenyuk, A.: Experimental determination of chemical diffusion within secondary organic aerosol particles, Phys. Chem. Chem. Phys., 15, 2983-2991, 10.1039/c2cp44013j, 2013.

Bahreini, R., Keywood, M. D., Ng, N. L., Varutbangkul, V., Gao, S., Flagan, R. C., Seinfeld, J. H., Worsnop, D. R., and Jimenez, J. L.: Measurements of Secondary Organic Aerosol from Oxidation of Cycloalkenes, Terpenes, and m-Xylene Using an Aerodyne Aerosol Mass Spectrometer, Environmental Science & Technology, 39, 5674-5688, 10.1021/es048061a, 2005.

Boyd, C. M., Sanchez, J., Xu, L., Eugene, A. J., Nah, T., Tuet, W. Y., Guzman, M. I., and Ng, N. L.: Secondary organic aerosol formation from the β-pinene+NO3 system: effect of humidity and peroxy radical fate, Atmos. Chem. Phys., 15, 7497-7522, 10.5194/acp-15-7497-2015, 2015.

Canagaratna, M. R., Jimenez, J. L., Kroll, J. H., Chen, Q., Kessler, S. H., Massoli, P., Hildebrandt Ruiz, L., Fortner, E., Williams, L. R., Wilson, K. R., Surratt, J. D., Donahue, N. M., Jayne, J. T., and Worsnop, D. R.: Elemental ratio measurements of organic compounds using aerosol mass spectrometry: characterization, improved calibration, and implications, Atmos. Chem. Phys., 15, 253-272, 10.5194/acp-15-253-2015, 2015.

Capouet, M., Müller, J. F., Ceulemans, K., Compernolle, S., Vereecken, L., and Peeters, J.: Modeling aerosol formation in alpha-pinene photo-oxidation experiments, Journal of Geophysical Research: Atmospheres, 113, n/a-n/a, 10.1029/2007JD008995, 2008.

Cappa, C. D., and Wilson, K. R.: Evolution of organic aerosol mass spectra upon heating: implications for OA phase and partitioning behavior, Atmospheric Chemistry and Physics, 11, 1895-1911, 10.5194/acp-11-1895-2011, 2011.

871 Cappa, C. D., Jathar, S. H., Kleeman, M. J., Docherty, K. S., Jimenez, J. L., Seinfeld, J.
872 H., and Wexler, A. S.: Simulating secondary organic aerosol in a regional air quality
873 model using the statistical oxidation model – Part 2: Assessing the influence of vapor
874 wall losses, Atmos. Chem. Phys., 16, 3041-3059, 10.5194/acp-16-3041-2016, 2016.

875 Carlton, A. G., Bhave, P. V., Napelenok, S. L., Edney, E. D., Sarwar, G., Pinder, R. W.,
876 Pouliot, G. A., and Houyoux, M.: Model Representation of Secondary Organic Aerosol in
877 CMAQv4.7, Environmental Science & Technology, 44, 8553-8560, 10.1021/es100636q,
878 2010.

879 Chan, A. W. H., Kroll, J. H., Ng, N. L., and Seinfeld, J. H.: Kinetic modeling of
880 secondary organic aerosol formation: effects of particle- and gas-phase reactions of
881 semivolatile products, Atmospheric Chemistry and Physics, 7, 4135-4147, 2007.

882 Cocker, D. R., Flagan, R. C., and Seinfeld, J. H.: State-of-the-art chamber facility for
883 studying atmospheric aerosol chemistry, Environmental Science & Technology, 35,
884 2594-2601, 10.1021/es0019169, 2001a.

885 Cocker, D. R., Clegg, S. L., Flagan, R. C., and Seinfeld, J. H.: The effect of water on gas-
886 particle partitioning of secondary organic aerosol. Part I: alpha-pinene/ozone system,
887 Atmospheric Environment, 35, 6049-6072, 10.1016/s1352-2310(01)00404-6, 2001b.

888 Crounse, J. D., Nielsen, L. B., Jorgensen, S., Kjaergaard, H. G., and Wennberg, P. O.:
889 Autoxidation of Organic Compounds in the Atmosphere, J. Phys. Chem. Lett., 4, 3513-
890 3520, 10.1021/jz4019207, 2013.

891 Crump, J. G., and Seinfeld, J. H.: Turbulent Deposition and Gravitational Sedimentation
892 of an Aerosol in a Vessel of Arbitrary Shape, Journal of Aerosol Science, 12, 405-415,
893 10.1016/0021-8502(81)90036-7, 1981.

894 DeCarlo, P. F., Slowik, J. G., Worsnop, D. R., Davidovits, P., and Jimenez, J. L.: Particle
895 morphology and density characterization by combined mobility and aerodynamic
896 diameter measurements. Part 1: Theory, Aerosol Sci. Technol., 38, 1185-1205,
897 10.1080/027868290903907, 2004.

898 DeCarlo, P. F., Kimmel, J. R., Trimborn, A., Northway, M. J., Jayne, J. T., Aiken, A. C.,
899 Gonin, M., Fuhrer, K., Horvath, T., Docherty, K. S., Worsnop, D. R., and Jimenez, J. L.:
900 Field-deployable, high-resolution, time-of-flight aerosol mass spectrometer, Analytical
901 Chemistry, 78, 8281-8289, 10.1021/ac061249n, 2006.

902 Docherty, K. S., Wu, W., Lim, Y. B., and Ziemann, P. J.: Contributions of organic
903 peroxides to secondary aerosol formed from reactions of monoterpenes with O3,
904 Environmental Science & Technology, 39, 4049-4059, 10.1021/es050228s, 2005.

905 Donahue, N. M., Robinson, A. L., Stanier, C. O., and Pandis, S. N.: Coupled partitioning,
906 dilution, and chemical aging of semivolatile organics, Environmental Science &
907 Technology, 40, 2635-2643, 10.1021/es052297c, 2006.

908 Donahue, N. M., Epstein, S. A., Pandis, S. N., and Robinson, A. L.: A two-dimensional
909 volatility basis set: 1. organic-aerosol mixing thermodynamics, Atmospheric Chemistry
910 and Physics, 11, 3303-3318, 10.5194/acp-11-3303-2011, 2011.

911 Ehn, M., Thornton, J. A., Kleist, E., Sipila, M., Junninen, H., Pullinen, I., Springer, M.,
912 Rubach, F., Tillmann, R., Lee, B., Lopez-Hilfiker, F., Andres, S., Acir, I. H., Rissanen,
913 M., Jokinen, T., Schobesberger, S., Kangasluoma, J., Kontkanen, J., Nieminen, T.,
914 Kurten, T., Nielsen, L. B., Jorgensen, S., Kjaergaard, H. G., Canagaratna, M., Dal Maso,
915 M., Berndt, T., Petaja, T., Wahner, A., Kerminen, V. M., Kulmala, M., Worsnop, D. R.,
916 Wildt, J., and Mentel, T. F.: A large source of low-volatility secondary organic aerosol,
917 Nature, 506, 476-479, 10.1038/nature13032, 2014.

918 Fry, J. L., Kiendler-Scharr, A., Rollins, A. W., Wooldridge, P. J., Brown, S. S., Fuchs,
919 H., Dube, W., Mensah, A., dal Maso, M., Tillmann, R., Dorn, H. P., Brauers, T., and
920 Cohen, R. C.: Organic nitrate and secondary organic aerosol yield from NO3 oxidation of
921 beta-pinene evaluated using a gas-phase kinetics/aerosol partitioning model, Atmospheric
922 Chemistry and Physics, 9, 1431-1449, 2009.

923 Fry, J. L., Draper, D. C., Barsanti, K. C., Smith, J. N., Ortega, J., Winkler, P. M., Lawler,
924 M. J., Brown, S. S., Edwards, P. M., Cohen, R. C., and Lee, L.: Secondary Organic
925 Aerosol Formation and Organic Nitrate Yield from NO3 Oxidation of Biogenic

926 Hydrocarbons, Environmental Science & Technology, 48, 11944-11953,
927 10.1021/es502204x, 2014.

928 Gao, S., Ng, N. L., Keywood, M., Varutbangkul, V., Bahreini, R., Nenes, A., He, J. W.,
929 Yoo, K. Y., Beauchamp, J. L., Hodyss, R. P., Flagan, R. C., and Seinfeld, J. H.: Particle
930 phase acidity and oligomer formation in secondary organic aerosol, Environmental
931 Science & Technology, 38, 6582-6589, 10.1021/es049125k, 2004.

932 Grieshop, A. P., Donahue, N. M., and Robinson, A. L.: Is the gas-particle partitioning in
933 alpha-pinene secondary organic aerosol reversible?, Geophys. Res. Lett., 34, n/a-n/a,
934 10.1029/2007GL029987, 2007.

935 Griffin, R. J., Cocker, D. R., Flagan, R. C., and Seinfeld, J. H.: Organic aerosol formation
936 from the oxidation of biogenic hydrocarbons, J. Geophys. Res.-Atmos., 104, 3555-3567,
937 10.1029/1998jd100049, 1999.

938 Guenther, A. B., Jiang, X., Heald, C. L., Sakulyanontvittaya, T., Duhl, T., Emmons, L.
939 K., and Wang, X.: The Model of Emissions of Gases and Aerosols from Nature version
940 2.1 (MEGAN2.1): an extended and updated framework for modeling biogenic emissions,
941 Geoscientific Model Development, 5, 1471-1492, 10.5194/gmd-5-1471-2012, 2012.

942 Hallquist, M., Wenger, J. C., Baltensperger, U., Rudich, Y., Simpson, D., Claeys, M.,
943 Dommen, J., Donahue, N. M., George, C., Goldstein, A. H., Hamilton, J. F., Herrmann,
944 H., Hoffmann, T., Iinuma, Y., Jang, M., Jenkin, M. E., Jimenez, J. L., Kiendler-Scharr,
945 A., Maenhaut, W., McFiggans, G., Mentel, T. F., Monod, A., Prevot, A. S. H., Seinfeld,
946 J. H., Surratt, J. D., Szmigielski, R., and Wildt, J.: The formation, properties and impact
947 of secondary organic aerosol: current and emerging issues, Atmospheric Chemistry and
948 Physics, 9, 5155-5236, 2009.

949 Henry, K. M., Lohaus, T., and Donahue, N. M.: Organic Aerosol Yields from alpha-
950 Pinene Oxidation: Bridging the Gap between First-Generation Yields and Aging
951 Chemistry, Environmental Science & Technology, 46, 12347-12354, 10.1021/es302060y,
952 2012.

953 Hildebrandt, L., Donahue, N. M., and Pandis, S. N.: High formation of secondary organic
954 aerosol from the photo-oxidation of toluene, Atmospheric Chemistry and Physics, 9,
955 2973-2986, 2009.

956 Hoffmann, T., Odum, J. R., Bowman, F., Collins, D., Klockow, D., Flagan, R. C., and
957 Seinfeld, J. H.: Formation of organic aerosols from the oxidation of biogenic
958 hydrocarbons, Journal of Atmospheric Chemistry, 26, 189-222,
959 10.1023/a:1005734301837, 1997.

960 Kanakidou, M., Seinfeld, J. H., Pandis, S. N., Barnes, I., Dentener, F. J., Facchini, M. C.,
961 Van Dingenen, R., Ervens, B., Nenes, A., Nielsen, C. J., Swietlicki, E., Putaud, J. P.,
962 Balkanski, Y., Fuzzi, S., Horth, J., Moortgat, G. K., Winterhalter, R., Myhre, C. E. L.,
963 Tsigaridis, K., Vignati, E., Stephanou, E. G., and Wilson, J.: Organic aerosol and global
964 climate modelling: a review, Atmospheric Chemistry and Physics, 5, 1053-1123, 2005.

965 Karnezi, E., Riipinen, I., and Pandis, S. N.: Measuring the atmospheric organic aerosol
966 volatility distribution: a theoretical analysis, Atmospheric Measurement Techniques, 7,
967 2953—2965, 2014.

968 Keywood, M. D., Varutbangkul, V., Bahreini, R., Flagan, R. C., and Seinfeld, J. H.:
969 Secondary organic aerosol formation from the ozonolysis of cycloalkenes and related
970 compounds, Environmental Science & Technology, 38, 4157-4164, 10.1021/es035363o,
971 2004.

972 Kokkola, H., Yli-Pirila, P., Vesterinen, M., Korhonen, H., Keskinen, H., Romakkaniemi,
973 S., Hao, L., Kortelainen, A., Joutsensaari, J., Worsnop, D. R., Virtanen, A., and Lehtinen,
974 K. E. J.: The role of low volatile organics on secondary organic aerosol formation,
975 Atmospheric Chemistry and Physics, 14, 1689-1700, 10.5194/acp-14-1689-2014, 2014.

976 Kostenidou, E., Pathak, R. K., and Pandis, S. N.: An algorithm for the calculation of
977 secondary organic aerosol density combining AMS and SMPS data, Aerosol Sci.
978 Technol., 41, 1002-1010, 10.1080/02786820701666270, 2007.

979 Krechmer, J. E., Pagonis, D., Ziemann, P. J., and Jimenez, J. L.: Quantification of Gas-
980 Wall Partitioning in Teflon Environmental Chambers Using Rapid Bursts of Low-

Volatility Oxidized Species Generated in Situ, Environmental Science & Technology, 50, 5757-5765, 10.1021/acs.est.6b00606, 2016.

Kristensen, K., Cui, T., Zhang, H., Gold, A., Glasius, M., and Surratt, J. D.: Dimers in alpha-pinene secondary organic aerosol: effect of hydroxyl radical, ozone, relative humidity and aerosol acidity, Atmospheric Chemistry and Physics, 14, 4201-4218, 10.5194/acp-14-4201-2014, 2014.

Kroll, J. H., Chan, A. W. H., Ng, N. L., Flagan, R. C., and Seinfeld, J. H.: Reactions of semivolatile organics and their effects on secondary organic aerosol formation, Environmental Science & Technology, 41, 3545-3550, 10.1021/es062059x, 2007.

Kuwata, M., and Martin, S. T.: Phase of atmospheric secondary organic material affects its reactivity, Proc. Natl. Acad. Sci. U. S. A., 109, 17354-17359, 10.1073/pnas.1209071109, 2012.

La, Y. S., Camredon, M., Ziemann, P. J., Valorso, R., Matsunaga, A., Lannuque, V., Lee-Taylor, J., Hodzic, A., Madronich, S., and Aumont, B.: Impact of chamber wall loss of gaseous organic compounds on secondary organic aerosol formation: explicit modeling of SOA formation from alkane and alkene oxidation, Atmos. Chem. Phys., 16, 1417-1431, 10.5194/acp-16-1417-2016, 2016.

Loza, C. L., Chan, A. W. H., Galloway, M. M., Keutsch, F. N., Flagan, R. C., and Seinfeld, J. H.: Characterization of Vapor Wall Loss in Laboratory Chambers, Environmental Science & Technology, 44, 5074-5078, 10.1021/es100727v, 2010.

Loza, C. L., Chhabra, P. S., Yee, L. D., Craven, J. S., Flagan, R. C., and Seinfeld, J. H.: Chemical aging of m-xylene secondary organic aerosol: laboratory chamber study, Atmospheric Chemistry and Physics, 12, 151-167, 10.5194/acp-12-151-2012, 2012.

Matsunaga, A., and Ziemann, P. J.: Gas-Wall Partitioning of Organic Compounds in a Teflon Film Chamber and Potential Effects on Reaction Product and Aerosol Yield Measurements, Aerosol Sci. Technol., 44, 881-892, 10.1080/02786826.2010.501044, 2010.

1008 McMurry, P. H., and Grosjean, D.: Gas and Aerosol Wall Losses in Teflon Film Smog
1009 Chambers, Environmental Science & Technology, 19, 1176-1182, 10.1021/es00142a006,
1010 1985.

1011 McMurry, P. H., and Rader, D. J.: Aerosol Wall Losses in Electrically Charged
1012 Chambers, Aerosol Sci. Technol., 4, 249-268, 10.1080/02786828508959054, 1985.

1013 McVay, R. C., Cappa, C. D., and Seinfeld, J. H.: Vapor-Wall Deposition in Chambers:
1014 Theoretical Considerations, Environmental Science & Technology, 48, 10251-10258,
1015 10.1021/es502170j, 2014.

1016 McVay, R. C., Zhang, X., Aumont, B., Valorso, R., Camredon, M., La, Y. S., Wennberg,
1017 P. O., and Seinfeld, J. H.: SOA formation from the photooxidation of α-pinene:
1018 systematic exploration of the simulation of chamber data, Atmos. Chem. Phys., 16, 2785-
1019 2802, 10.5194/acp-16-2785-2016, 2016.

1020 Miles, R. E. H., Reid, J. P., and Riipinen, I.: Comparison of Approaches for Measuring
1021 the Mass Accommodation Coefficient for the Condensation of Water and Sensitivities to
1022 Uncertainties in Thermophysical Properties, J. Phys. Chem. A, 116, 10810-10825,
1023 10.1021/jp3083858, 2012.

1024 Ng, N. L., Kroll, J. H., Keywood, M. D., Bahreini, R., Varutbangkul, V., Flagan, R. C.,
1025 Seinfeld, J. H., Lee, A., and Goldstein, A. H.: Contribution of first- versus second-
1026 generation products to secondary organic aerosols formed in the oxidation of biogenic
1027 hydrocarbons, Environmental Science & Technology, 40, 2283-2297,
1028 10.1021/es052269u, 2006.

1029 Ng, N. L., Kroll, J. H., Chan, A. W. H., Chhabra, P. S., Flagan, R. C., and Seinfeld, J. H.:
1030 Secondary organic aerosol formation from m-xylene, toluene, and benzene, Atmospheric
1031 Chemistry and Physics, 7, 3909-3922, 2007.

1032 Odum, J. R., Hoffmann, T., Bowman, F., Collins, D., Flagan, R. C., and Seinfeld, J. H.:
1033 Gas/Particle Partitioning and Secondary Organic Aerosol Yields, Environmental Science
1034 & Technology, 30, 2580-2585, 10.1021/es950943+, 1996.

1035 Odum, J. R., Jungkamp, T. P. W., Griffin, R. J., Flagan, R. C., and Seinfeld, J. H.: The
1036 atmospheric aerosol-forming potential of whole gasoline vapor, Science, 276, 96-99,
1037 10.1126/science.276.5309.96, 1997a.

1038 Odum, J. R., Jungkamp, T. P. W., Griffin, R. J., Forstner, H. J. L., Flagan, R. C., and
1039 Seinfeld, J. H.: Aromatics, reformulated gasoline, and atmospheric organic aerosol
1040 formation, Environmental Science & Technology, 31, 1890-1897, 10.1021/es960535l,
1041 1997b.

1042 Pathak, R. K., Presto, A. A., Lane, T. E., Stanier, C. O., Donahue, N. M., and Pandis, S.
1043 N.: Ozonolysis of alpha-pinene: parameterization of secondary organic aerosol mass
1044 fraction, Atmospheric Chemistry and Physics, 7, 3811-3821, 2007a.

1045 Pathak, R. K., Stanier, C. O., Donahue, N. M., and Pandis, S. N.: Ozonolysis of alpha-
1046 pinene at atmospherically relevant concentrations: Temperature dependence of aerosol
1047 mass fractions (yields), J. Geophys. Res.-Atmos., 112, 8, 10.1029/2006jd007436, 2007b.

1048 Perraud, V., Bruns, E. A., Ezell, M. J., Johnson, S. N., Yu, Y., Alexander, M. L.,
1049 Zelenyuk, A., Imre, D., Chang, W. L., Dabdub, D., Pankow, J. F., and Finlayson-Pitts, B.
1050 J.: Nonequilibrium atmospheric secondary organic aerosol formation and growth, Proc.
1051 Natl. Acad. Sci. U. S. A., 109, 2836-2841, 10.1073/pnas.1119909109, 2012.

1052 Pierce, J. R., Engelhart, G. J., Hildebrandt, L., Weitkamp, E. A., Pathak, R. K., Donahue,
1053 N. M., Robinson, A. L., Adams, P. J., and Pandis, S. N.: Constraining particle evolution
1054 from wall losses, coagulation, and condensation-evaporation in smog-chamber
1055 experiments: Optimal estimation based on size distribution measurements, Aerosol Sci.
1056 Technol., 42, 1001-1015, 10.1080/02786820802389251, 2008.

1057 Presto, A. A., Hartz, K. E. H., and Donahue, N. M.: Secondary organic aerosol
1058 production from terpene ozonolysis. 2. Effect of NOx concentration, Environmental
1059 Science & Technology, 39, 7046-7054, 10.1021/es050400s, 2005.

1060 Presto, A. A., and Donahue, N. M.: Investigation of alpha-pinene plus ozone secondary
1061 organic aerosol formation at low total aerosol mass, Environmental Science &
1062 Technology, 40, 3536-3543, 10.1021/es052203z, 2006.

1063 Pye, H. O. T., Chan, A. W. H., Barkley, M. P., and Seinfeld, J. H.: Global modeling of
1064 organic aerosol: the importance of reactive nitrogen (NOx and NO3), Atmospheric
1065 Chemistry and Physics, 10, 11261-11276, 10.5194/acp-10-11261-2010, 2010.

1066 Renbaum-Wolff, L., Grayson, J. W., Bateman, A. P., Kuwata, M., Sellier, M., Murray, B.
1067 J., Shilling, J. E., Martin, S. T., and Bertram, A. K.: Viscosity of alpha-pinene secondary
1068 organic material and implications for particle growth and reactivity, Proc. Natl. Acad.
1069 Sci. U. S. A., 110, 8014-8019, 10.1073/pnas.1219548110, 2013.

1070 Saha, P. K., and Grieshop, A. P.: Exploring Divergent Volatility Properties from Yield
1071 and Thermodenuder Measurements of Secondary Organic Aerosol from α-Pinene
1072 Ozonolysis, Environmental Science & Technology, 50, 5740-5749,
1073 10.1021/acs.est.6b00303, 2016.

1074 Saleh, R., Donahue, N. M., and Robinson, A. L.: Time Scales for Gas-Particle
1075 Partitioning Equilibration of Secondary Organic Aerosol Formed from Alpha-Pinene
1076 Ozonolysis, Environmental Science & Technology, 47, 5588-5594, 10.1021/es400078d,
1077 2013.

1078 Saukko, E., Lambe, A. T., Massoli, P., Koop, T., Wright, J. P., Croasdale, D. R.,
1079 Pedernera, D. A., Onasch, T. B., Laaksonen, A., Davidovits, P., Worsnop, D. R., and
1080 Virtanen, A.: Humidity-dependent phase state of SOA particles from biogenic and
1081 anthropogenic precursors, Atmospheric Chemistry and Physics, 12, 7517-7529,
1082 10.5194/acp-12-7517-2012, 2012.

1083 Saunders, S. M., Jenkin, M. E., Derwent, R. G., and Pilling, M. J.: Protocol for the
1084 development of the Master Chemical Mechanism, MCM v3 (Part A): tropospheric
1085 degradation of non-aromatic volatile organic compounds, Atmos. Chem. Phys., 3, 161-
1086 180, 10.5194/acp-3-161-2003, 2003.

1087 Seinfeld, J. H., and Pandis, S. N.: Atmospheric chemistry and physics : from air pollution
1088 to climate change, 2nd ed., Wiley, Hoboken, N.J., xxviii, 1203 p. pp., 2006.

1089 Shilling, J. E., Chen, Q., King, S. M., Rosenoern, T., Kroll, J. H., Worsnop, D. R.,
1090 McKinney, K. A., and Martin, S. T.: Particle mass yield in secondary organic aerosol

formed by the dark ozonolysis of alpha-pinene, Atmospheric Chemistry and Physics, 8, 2073-2088, 2008.

Shilling, J. E., Chen, Q., King, S. M., Rosenoern, T., Kroll, J. H., Worsnop, D. R., DeCarlo, P. F., Aiken, A. C., Sueper, D., Jimenez, J. L., and Martin, S. T.: Loading-dependent elemental composition of alpha-pinene SOA particles, Atmospheric Chemistry and Physics, 9, 771-782, 2009.

Shiraiwa, M., and Seinfeld, J. H.: Equilibration timescale of atmospheric secondary organic aerosol partitioning, Geophys. Res. Lett., 39, 6, 10.1029/2012gl054008, 2012.

Song, C., Zaveri, R. A., Alexander, M. L., Thornton, J. A., Madronich, S., Ortega, J. V., Zelenyuk, A., Yu, X. Y., Laskin, A., and Maughan, D. A.: Effect of hydrophobic primary organic aerosols on secondary organic aerosol formation from ozonolysis of alpha-pinene, Geophys. Res. Lett., 34, 5, 10.1029/2007gl030720, 2007.

Stanier, C. O., Pathak, R. K., and Pandis, S. N.: Measurements of the volatility of aerosols from alpha-piniene ozonolysis, Environmental Science & Technology, 41, 2756-2763, 10.1021/es0519280, 2007.

Tabge, O. GNU Parallel – The Command-Line Power Tool, :login: The USENIX Magazine, http://www.gnu.org/s/parallel, 2011.

Tsigaridis, K., Daskalakis, N., Kanakidou, M., Adams, P. J., Artaxo, P., Bahadur, R., Balkanski, Y., Bauer, S. E., Bellouin, N., Benedetti, A., Bergman, T., Berntsen, T. K., Beukes, J. P., Bian, H., Carslaw, K. S., Chin, M., Curci, G., Diehl, T., Easter, R. C., Ghan, S. J., Gong, S. L., Hodzic, A., Hoyle, C. R., Iversen, T., Jathar, S., Jimenez, J. L., Kaiser, J. W., Kirkevåg, A., Koch, D., Kokkola, H., Lee, Y. H., Lin, G., Liu, X., Luo, G., Ma, X., Mann, G. W., Mihalopoulos, N., Morcrette, J. J., Müller, J. F., Myhre, G., Myriokefalitakis, S., Ng, N. L., O'Donnell, D., Penner, J. E., Pozzoli, L., Pringle, K. J., Russell, L. M., Schulz, M., Sciare, J., Seland, Ø., Shindell, D. T., Sillman, S., Skeie, R. B., Spracklen, D., Stavrakou, T., Steenrod, S. D., Takemura, T., Tiitta, P., Tilmes, S., Tost, H., van Noije, T., van Zyl, P. G., von Salzen, K., Yu, F., Wang, Z., Wang, Z., Zaveri, R. A., Zhang, H., Zhang, K., Zhang, Q., and Zhang, X.: The AeroCom evaluation

1119 and intercomparison of organic aerosol in global models, Atmos. Chem. Phys., 14,
1120 10845-10895, 10.5194/acp-14-10845-2014, 2014.

1121 Vaden, T. D., Song, C., Zaveri, R. A., Imre, D., and Zelenyuk, A.: Morphology of mixed
1122 primary and secondary organic particles and the adsorption of spectator organic gases
1123 during aerosol formation, Proc. Natl. Acad. Sci. U. S. A., 107, 6658-6663,
1124 10.1073/pnas.0911206107, 2010.

1125 Vaden, T. D., Imre, D., Beranek, J., Shrivastava, M., and Zelenyuk, A.: Evaporation
1126 kinetics and phase of laboratory and ambient secondary organic aerosol, Proc. Natl.
1127 Acad. Sci. U. S. A., 108, 2190-2195, 10.1073/pnas.1013391108, 2011.

1128 Virtanen, A., Joutsensaari, J., Koop, T., Kannosto, J., Yli-Pirila, P., Leskinen, J., Makela,
1129 J. M., Holopainen, J. K., Poschl, U., Kulmala, M., Worsnop, D. R., and Laaksonen, A.:
1130 An amorphous solid state of biogenic secondary organic aerosol particles, Nature, 467,
1131 824-827, 10.1038/nature09455, 2010.

1132 Virtanen, A., Kannosto, J., Kuuluvainen, H., Arffman, A., Joutsensaari, J., Saukko, E.,
1133 Hao, L., Yli-Pirila, P., Tiitta, P., Holopainen, J. K., Keskinen, J., Worsnop, D. R., Smith,
1134 J. N., and Laaksonen, A.: Bounce behavior of freshly nucleated biogenic secondary
1135 organic aerosol particles, Atmospheric Chemistry and Physics, 11, 8759-8766,
1136 10.5194/acp-11-8759-2011, 2011.

1137 Weitkamp, E. A., Sage, A. M., Pierce, J. R., Donahue, N. M., and Robinson, A. L.:
1138 Organic aerosol formation from photochemical oxidation of diesel exhaust in a smog
1139 chamber, Environmental Science & Technology, 41, 6969-6975, 10.1021/es070193r,
1140 2007.

1141 Yeh, G. K., and Ziemann, P. J.: Alkyl Nitrate Formation from the Reactions of C-8-C-14
1142 n-Alkanes with OH Radicals in the Presence of NOx: Measured Yields with Essential
1143 Corrections for Gas-Wall Partitioning, J. Phys. Chem. A, 118, 8147-8157,
1144 10.1021/jp500631v, 2014.

1145 Yeh, G. K., and Ziemann, P. J.: Gas-Wall Partitioning of Oxygenated Organic
1146 Compounds: Measurements, Structure-Activity Relationships, and Correlation with Gas

1147 Chromatographic Retention Factor, Aerosol Sci. Technol., 49, 726-737,
1148 10.1080/02786826.2015.1068427, 2015.

1149 Ye, P., Ding, X., Hakala, J., Hofbauer, V., Robinson, E. S., and Donahue, N. M.: Vapor
1150 wall loss of semi-volatile organic compounds in a Teflon chamber, Aerosol Sci. Technol.,
1151 50, 822-834, 10.1080/02786826.2016.1195905, 2016.

1152 Zaveri, R. A., Easter, R. C., Shilling, J. E., and Seinfeld, J. H.: Modeling kinetic
1153 partitioning of secondary organic aerosol and size distribution dynamics: representing
1154 effects of volatility, phase state, and particle-phase reaction, Atmospheric Chemistry and
1155 Physics, 14, 5153-5181, 10.5194/acp-14-5153-2014, 2014.

1156 Zhang, X., Pandis, S. N., and Seinfeld, J. H.: Diffusion-Limited Versus Quasi-
1157 Equilibrium Aerosol Growth, Aerosol Sci. Technol., 46, 874-885,
1158 10.1080/02786826.2012.679344, 2012.

1159 Zhang, X., Cappa, C. D., Jathar, S. H., McVay, R. C., Ensberg, J. J., Kleeman, M. J., and
1160 Seinfeld, J. H.: Influence of vapor wall loss in laboratory chambers on yields of
1161 secondary organic aerosol, Proc. Natl. Acad. Sci. U. S. A., 111, 5802-5807,
1162 10.1073/pnas.1404727111, 2014.

1163 Zhang, X., Schwantes, R. H., McVay, R. C., Lignell, H., Coggon, M. M., Flagan, R. C.,
1164 and Seinfeld, J. H.: Vapor wall deposition in Teflon chambers, Atmospheric Chemistry
1165 and Physics, 15, 4197-4214, 10.5194/acp-15-4197-2015, 2015a.

1166 Zhang, X., McVay, R. C., Huang, D. D., Dalleska, N. F., Aumont, B., Flagan, R. C., and
1167 Seinfeld, J. H.: Formation and evolution of molecular products in alpha-pinene secondary
1168 organic aerosol, Proc. Natl. Acad. Sci. U. S. A., 112, 14168-14173,
1169 10.1073/pnas.1517742112, 2015b.

1170

1171

1172

Table 1: Experimental conditions and results for the α-pinene ozonolysis experiments

Experiment	Initial Seed Surface Area ($\mu m^2\ cm^{-3}$)	Initial [α-pinene][a] ($\mu g\ m^{-3}$)	ΔM_o[b] ($\mu g\ m^{-3}$)	SOA Mass Yield[c] (%)
100 ppb O_3 nucleation	0	290.2±23.2	62.0±1.2[d]	22.6±1.9
100 ppb O_3 low AS	1130	280.5±22.4	63.0±0.8[d]	23.3±1.9
100 ppb O_3 high AS	2700	238.7±19.1	50.6±1.6[d]	23.3±1.9
500 ppb O_3 nucleation	0	274.4±21.9	87.3±0.3[e]	31.8±2.5
500 ppb O_3 low AS	1300	264.9±21.2	75.7±0.6[e]	28.6±2.3
500 ppb O_3 high AS	2720	236.1±18.9	66.3±1.9[e]	28.1±2.4

[a]Concentration of α-pinene injected into the chamber. All the α-pinene reacted in the 500 ppb O_3 experiments, but not the 100 ppb O_3 experiments.

[b]Uncertainties in the peak SOA mass concentration (ΔM_o) are calculated from one standard deviation of the aerosol volume as measured by the scanning mobility particle sizer.

[c]SOA mass yields at peak SOA growth are reported.

[d]The SOA mass concentration is calculated using the density = 1.39 g cm^{-3} obtained from the 100 ppb O_3 nucleation experiment.

[e]The SOA mass concentration is calculated using the density = 1.37 g cm^{-3} obtained from the 500 ppb O_3 nucleation experiment.

Table 2: Coupled vapor-particle dynamics model parameters

Parameter	Definition	Value
α_p	Vapor-particle mass accommodation coefficient	0.1
α_w	Vapor-wall mass accommodation coefficient	10^{-6}
τ_{olig}	Timescale of oligomerization	4 h
C^*	Branching ratios and saturation concentrations of oxidation products	[0.6 (>10^3), 0.3(10^2), 0.05(10), 0.05(1) and 0(0.1)]
D_i	Gas-phase molecular diffusivity	3×10^{-6} m^2 s^{-1}
A/V	Surface area-to-volume ratio of the chamber	2.5 m^{-1}
C_w	Equivalent organic mass concentration in the wall	10 mg m^{-3}
k_e	Eddy diffusion coefficient	0.03 s^{-1}
M_i	Molecular weight of the diffusing gas-phase molecule i	168, 184, 192, 200 and 216 g mole^{-1}
M_{init}	Initially absorbing organic material in seed aerosol	0.01 μg m^{-3}
P	Pressure	1×10^5 Pa
T	Temperature	298 K
ρ_{seed}	Density of inorganic seed	1700 kg m^{-3}
ρ_{org}	Density of organic material on seed particle	1300 kg m^{-3}

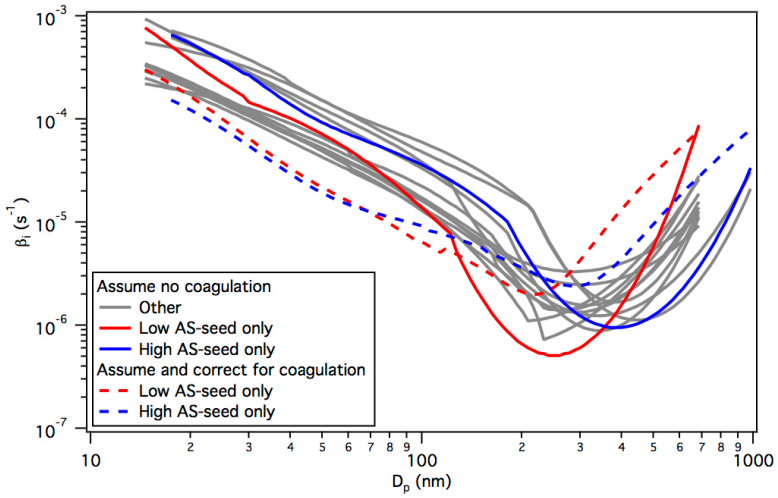

1204

1205 **Figure 1:** Particle wall deposition coefficients (β_i) measured during the low AS-seed
1206 only and high AS-seed only experiments in GTEC. Also shown are the particle wall
1207 deposition coefficients (labeled "Other") measured in previous routine monthly AS-seed
1208 only experiments in the chamber. These previous routine monthly AS-seed only
1209 experiments were performed using either a 0.008 M AS or a 0.1 M AS solution.
1210 Coagulation-corrected particle wall deposition coefficients (see Pierce et al. (2008) and
1211 main text for details) are also shown, using dashed lines.

1212

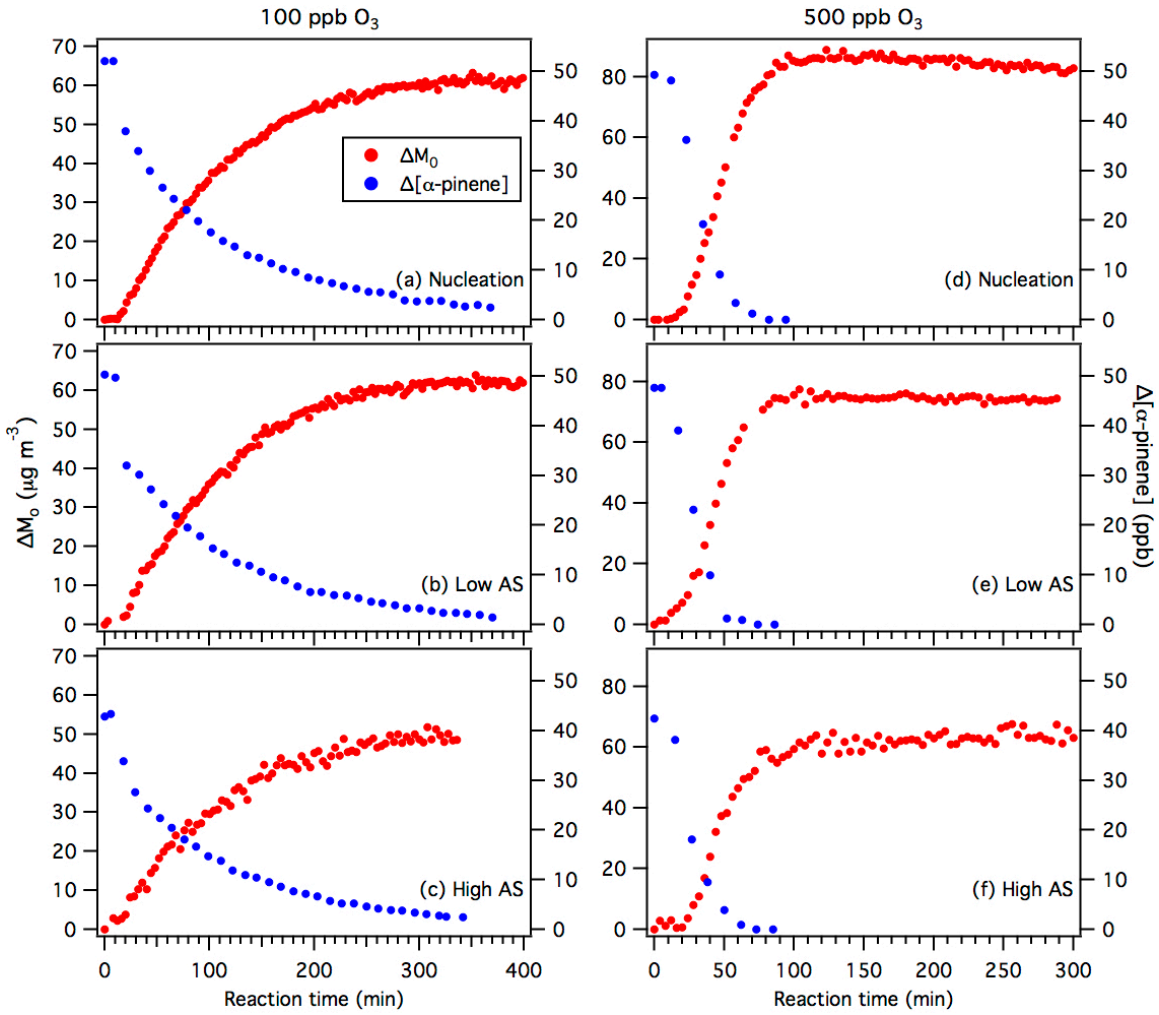

Figure 2: Reaction profiles of the α-pinene ozonolysis experiments. Panels (a), (b) and (c) show results from the nucleation, low AS and high AS 100 ppb O_3 experiments, respectively. Panels (d), (e) and (f) show results from the nucleation, low AS and high AS 500 ppb O_3 experiments, respectively. As explained in the main text, the SOA mass concentrations (ΔM_o) for the nucleation and low AS experiments are obtained using the particle wall deposition rates obtained from the low AS-seed only experiments, while the SOA mass concentrations (ΔM_o) for the high AS-seed experiments are obtained using the particle wall deposition rates obtained from the high AS-seed only experiments.

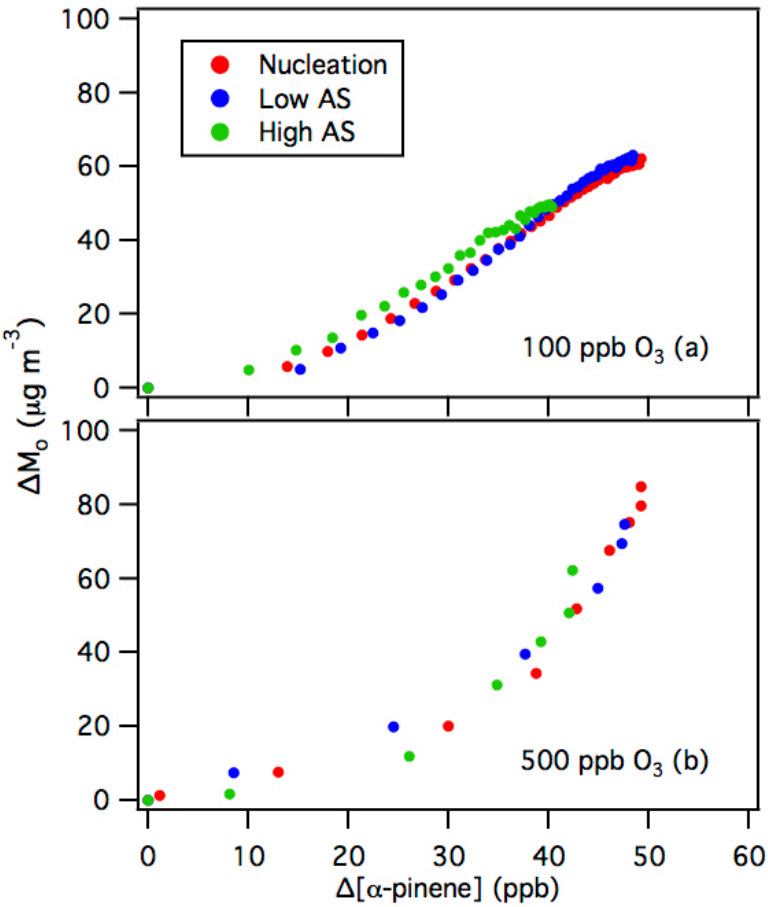

1223

1224 **Figure 3:** Time-dependent SOA growth curves for α-pinene ozonolysis. Panels (a) and
1225 (b) show 10 min-averaged results from the 100 ppb and 500 ppb O_3 experiments,
1226 respectively. Only SOA growth data up to the point of SOA peak growth are shown.

1227

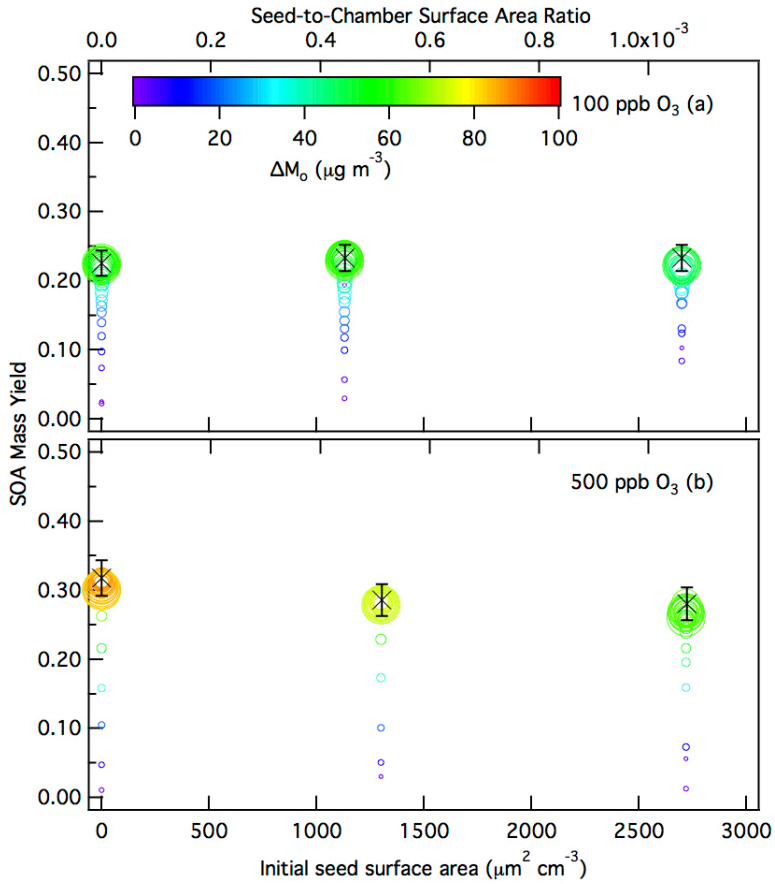

1228

1229 **Figure 4:** 10 min-averaged SOA mass yields over the course of an α-pinene ozonolysis
1230 experiment as a function of initial total AS seed surface area concentration for the (a) 100
1231 ppb O_3 experiments, and (b) 500 ppb O_3 experiments. Symbol color indicates the SOA
1232 mass concentration and symbol size indicates the time after O_3 is injected into the
1233 chamber. The × symbols are the SOA mass yields at peak SOA growth obtained from
1234 the experimental data. The y-axis error bars represent the uncertainty in the SOA mass
1235 yield at peak SOA growth, which originates from the α-pinene injection and the aerosol
1236 volume concentration measured by the SMPS at peak SOA growth (one standard
1237 deviation).

1238

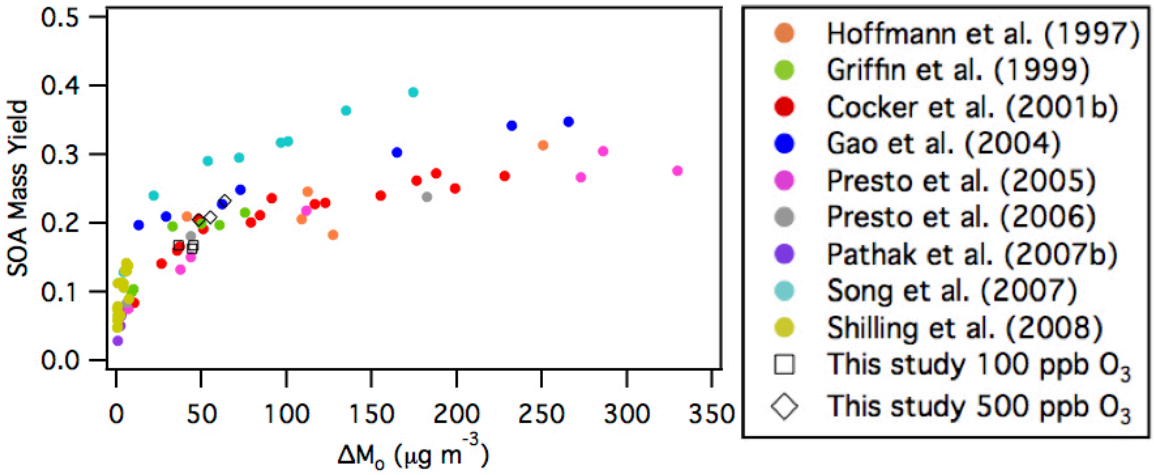

Figure 5: Comparison of SOA mass yields obtained in this study to those of previous dark α-pinene ozonolysis studies (Table S3). The SOA mass yields and concentrations of majority of these previous studies (Hoffmann et al., 1997; Griffin et al., 1999; Cocker et al., 2001b; Gao et al., 2004; Presto et al., 2005; Presto et al. 2006; Pathak et al., 2007b; Song et al., 2007) were previously compiled by Shilling et al. (2008). Similar to Shilling et al. (2008), all the data shown here (including those reported in this study) have been adjusted using an organic density of 1.0 g cm^{-3}, and to 298 K using a temperature correction of 1.6 % per K, as recommended by Pathak et al. (2007b) to facilitate easier comparison among the different studies.

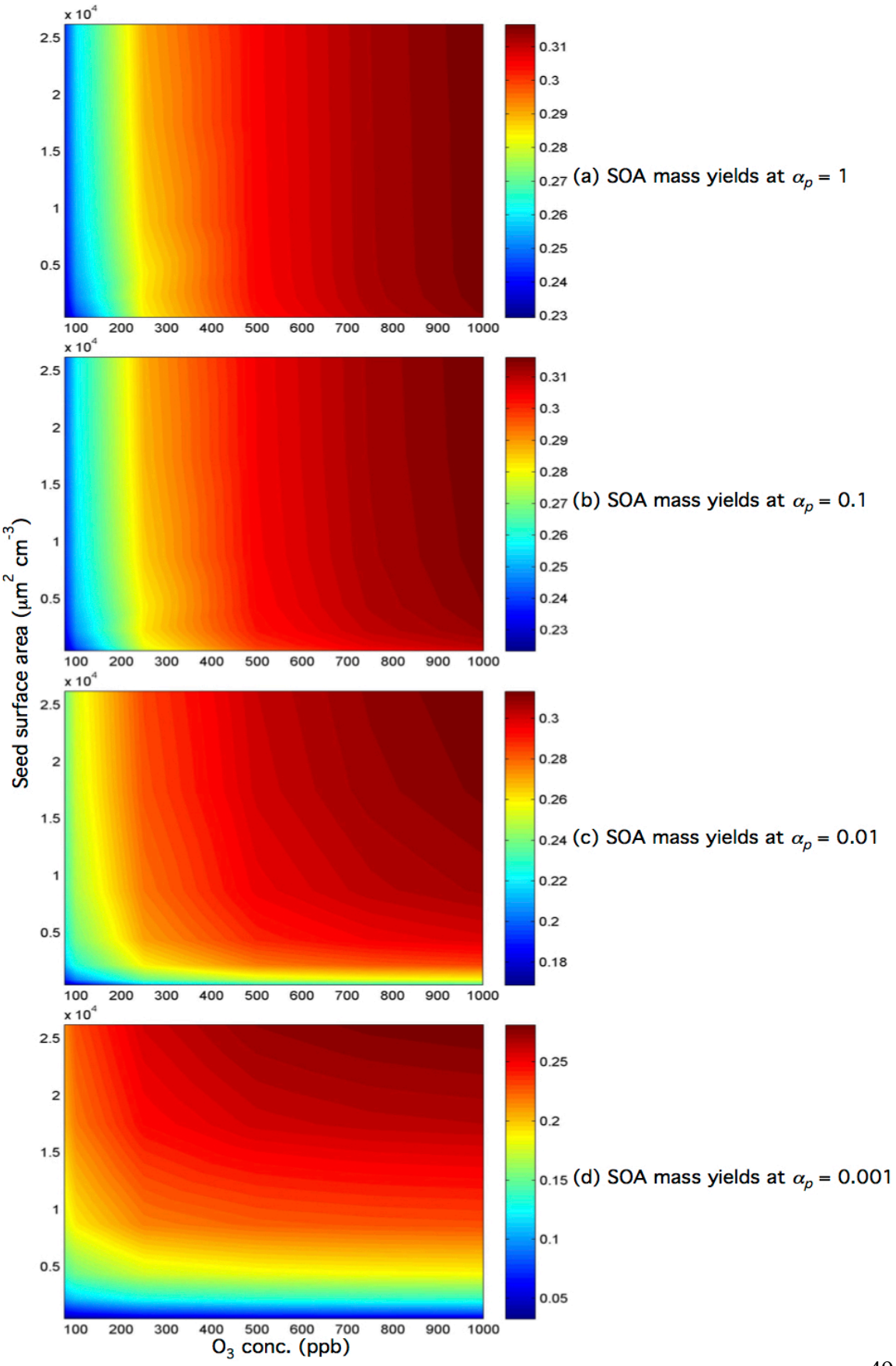
x 10^4
2.5
2
1.5
1
0.5
100 200 300 400 500 600 700 800 900 1000
0.31
0.3
0.29
0.28
0.27
0.26
0.25
0.24
0.23
(a) SOA mass yields at α_p = 1
(b) SOA mass yields at α_p = 0.1
0.22
0.2
0.18
(c) SOA mass yields at α_p = 0.01
0.15
0.1
0.05
(d) SOA mass yields at α_p = 0.001
Seed surface area (μm^2 cm^{-3})
O_3 conc. (ppb)

1250

Figure 6: SOA mass yields at peak SOA growth as a function of both the seed surface area and O_3 concentration for α_p = 1, 0.1, 0.01, and 0.001. The SOA mass yields at peak SOA growth are indicated by colors and contours. Note that the color bars for panels (a), (b) and (c) have different SOA mass yield ranges. Simulations were carried out using the optimal branching ratios, oligomerization rate, and vapor wall deposition rate parameters obtained in this study. The initial α-pinene concentration was set to 50 ppb, and a fixed O_3 concentration was used in place of a linear injection.